Miner Deposita (2012) 47:663–682
DOI 10.1007/s00126-011-0388-x

ARTICLE

Hydrocarbon- and ore-bearing basinal fluids: a possible link between gold mineralization and hydrocarbon accumulation in the Youjiang basin, South China

X. X. Gu · Y. M. Zhang · B. H. Li · S. Y. Dong · C. J. Xue · S. H. Fu

Received: 24 September 2010 / Accepted: 17 October 2011 / Published online: 6 November 2011

Abstract The Youjiang basin, which flanks the southwest edge of the Yangtze craton in South China, contains many Carlin-type gold deposits and abundant paleo-oil reservoirs. The gold deposits and paleo-oil reservoirs are restricted to the same tectonic units, commonly at the basinal margins and within the intrabasinal isolated platforms and/or bioherms. The gold deposits are hosted by Permian to Triassic carbonate and siliciclastic rocks that typically contain high contents of organic carbon. Paragenetic relationships indicate that most of the deposits exhibit an early stage of barren quartz±pyrite (stage I), a main stage of auriferous quartz+arsenian pyrite+arsenopyrite+marcasite (stage II), and a late stage of quartz+calcite+realgar± orpiment±native arsenic±stibnite±cinnabar±dolomite (stage III). Bitumen in the gold deposits is commonly present as a migrated hydrocarbon product in mineralized host rocks, particularly close to high grade ores, but is absent in barren sedimentary rocks. Bitumen dispersed in the mineralized rocks is closely associated and/or intergrown with the main stage jasperoidal quartz, arsenian pyrite, and arsenopyrite. Bitumen occurring in hydrothermal veins and veinlets is paragenetically associated with stages II and III mineral assemblages. These observations suggest an intimate relationship between bitumen precipitation and gold mineralization. In the paleo-petroleum reservoirs that typically occur in Permian reef limestones, bitumen is most commonly observed in open spaces, either alone or associated with calcite. Where bitumen occurs with calcite, it is typically concentrated along pore/vein centers as well as along the wall of pores and fractures, indicating approximately coeval precipitation. In the gold deposits, aqueous fluid inclusions are dominant in the early stage barren quartz veins (stage I), with a homogenization temperature range typically of 230°C to 270°C and a salinity range of 2.6 to 7.2 wt% NaCl eq. Fluid inclusions in the main and late-stage quartz and calcite are dominated by aqueous inclusions as well as hydrocarbon- and CO_2-rich inclusions. The presence of abundant hydrocarbon fluid inclusions in the gold deposits provides evidence that at least during main periods of the hydrothermal activity responsible for gold mineralization, the ore fluids consisted of an aqueous solution and an immiscible hydrocarbon phase. Aqueous inclusions in the main stage quartz associated with gold mineralization (stage II) typically have a homogenization temperature range of 200–230°C and a modal salinity around 5.3 wt% NaCl eq. Homogenization temperatures and salinities of aqueous inclusions in the late-stage drusy quartz and calcite (stage III) typically range from 120°C to 160°C and from 2.0 to 5.6 wt% NaCl eq., respectively. In the paleo-oil reservoirs, aqueous fluid inclusions with an average homogenization temperature of 80°C are dominant in early diagenetic calcite. Fluid

Editorial handling: N. C. White

X. X. Gu (✉) · Y. M. Zhang · C. J. Xue
State Key Laboratory of Geological Processes and Mineral Resources, China University of Geosciences,
Xueyuan Road 29,
Beijing 100083, China
e-mail: xuexiang_gu@cugb.edu.cn

X. X. Gu · S. H. Fu
State Key Laboratory of Ore Deposit Geochemistry,
Chinese Academy of Sciences,
Guanshui Road 79,
Guiyang 550002, China

B. H. Li · S. Y. Dong
College of Earth Sciences, Chengdu University of Technology,
Erxianqiao East Road 1,
Chengdu 610059, China

inclusions in late diagenetic pore- and fissure-filling calcite associated with bitumen are dominated by liquid C_2H_6, vapor CH_4, CH_4–H_2O, and aqueous inclusions, with a typical homogenization temperature range of 90°C to 180°C and a salinity range of 2–8 wt% NaCl eq. It is suggested that the hydrocarbons may have been trapped at relatively low temperatures, while the formation of gold deposits could have occurred under a wider and higher range of temperatures. The timing of gold mineralization in the Youjiang basin is still in dispute and a wide range of ages has been reported for individual deposits. Among the limited isotopic data, the Rb–Sr date of 206±12 Ma for Au-bearing hydrothermal sericite at Jinya as well as the Re–Os date of 193±13 Ma on auriferous arsenian pyrite and $^{40}Ar/^{39}Ar$ date of 194.6±2 Ma on vein-filling sericite at Lannigou may provide the most reliable age constraints on gold mineralization. This age range is comparable with the estimated petroleum charging age range of 238–185 Ma and the Sm–Nd date of 182±21 Ma for the pore- and fissure-filling calcite associated with bitumen at the Shitouzhai paleo-oil reservoir, corresponding to the late Indosinian to early Yanshanian orogenies in South China. The close association of Carlin-type gold deposits and paleo-oil reservoirs, the paragenetic coexistence of bitumens with ore-stage minerals, the presence of abundant hydrocarbons in the ore fluids, and the temporal coincidence of gold mineralization and hydrocarbon accumulation all support a coeval model in which the gold originated, migrated, and precipitated along with the hydrocarbons in an immiscible, gold- and hydrocarbon-bearing, basinal fluid system.

Keywords Gold mineralization · Hydrocarbon accumulation · Carlin-type gold deposit · Paleo-oil reservoir · Basinal fluid · Youjiang basin · China

Introduction

Sedimentary basins are important repositories for both energy fuels and many metals such as Pb, Zn, Cu, Au, and U. In the last two decades, the intimate association between metal deposits and hydrocarbon reservoirs (or fossil oil reservoirs) in a sedimentary basin has been widely noted. In general, metallic deposits closely associated with hydrocarbons include Mississippi Valley-type (MVT) Pb–Zn deposits in carbonate rocks (Montacer et al. 1988; Anderson 1991; Henry et al. 1992; Spirakis and Heyl 1992; Kesler et al. 1994; Eisenlohr et al. 1994; Gize and Barnes 1994; Spangenberg and Macko 1998; Mossman 1999; Lee and Williams 2000; Huston et al. 2006), manto-type Cu deposits in conglomerates or volcanic rocks (Wilson et al. 2003; Wilson and Zentilli 2006; Rieger et al. 2008), Cu and U deposits in sandstones and shales (Zhang 1994; Sun and Püttmann 2000; Cai et al. 2007), cinnabar deposits in black shales (Peabody and Einaudi 1992; Peabody 1993), and sedimentary-rock hosted Au, As, Hg, Sb, and Tl deposits (Radtke and Scheiner 1970; Hanor 1994; Gu 1996; Hulen and Collister 1999; Emsbo et al. 1999; Arehart 1996; Gu et al. 2002, 2007a).

On the regional scale, both ore deposits and hydrocarbon reservoirs or showings are commonly restricted to a same tectonic unit of the basin and controlled by similar structures, especially regional anticlines, domes, and paleohighs (Gu et al. 2007a). At the deposit, hand-sample, and microscopic scales, metallic ores are spatially associated with hydrocarbons. Organic matter in the deposits may occur in different forms, such as kerogen, bitumen, solid carbon, hydrocarbon gas, and even notable quantities of free oil in vugs, along fractures, and in fluid inclusions (e.g., Anderson 1991; Peabody 1993; Hulen and Collister 1999). In many cases, oil fields and overmature petroleum reservoirs are considered to be suitable sites for mineralization (Broadbent et al. 1998; Wilson and Zentilli 2006; Xue et al. 2007). In particular, concentrations of some metals (e.g., V, Ni, Mo, U, Cu, Pb, Zn, Au, Ag, As, Sb, and Hg) in crude oil, oil field brine, and solid bitumen may reach ore levels or even higher (Carpenter et al. 1974; Sverjensky 1984; Parnell 1988; Curiale 1993; Tu 1994; Farrell and Mossman 1994; Mossman 1999; Williams-Jones and Migdisov 2006).

The Youjiang basin in South China is characterized by containing many deposits of Sb, As, Hg, Tl, and barite, as well as a large number of sedimentary rock-hosted, disseminated Au deposits of Carlin-type (Liu et al. 2002; Hu et al. 2002; Gu et al. 2007a; Peters et al. 2007; Fig. 1). The basin is also well known as an important host to abundant fossil oil reservoirs and has attracted wide attention from petroleum geologists (Zhuang et al. 1999; Zhao et al. 2007; Gu et al. 2007a). The ore deposits show a close spatial association with paleo-petroleum reservoirs, suggesting a genetic link between mineralization and hydrocarbon accumulation. The major purpose of this paper is to examine the paragenetic relationships between hydrothermal minerals and hydrocarbons and to document the fluid characteristics of some Carlin-type Au deposits and paleo-reservoirs from the Youjiang basin to provide an insight into their formation and evolution, as well as into the mechanism of gold mineralization and hydrocarbon accumulation.

Geological setting

The Youjiang basin lies along the southwest margin of the Yangtze craton, at the border of Yunnan, Guizhou, and Guangxi provinces in southwest China (Fig. 1). The basin developed on lower Paleozoic basement and has experienced three distinctive stages since the late Paleozoic: rift

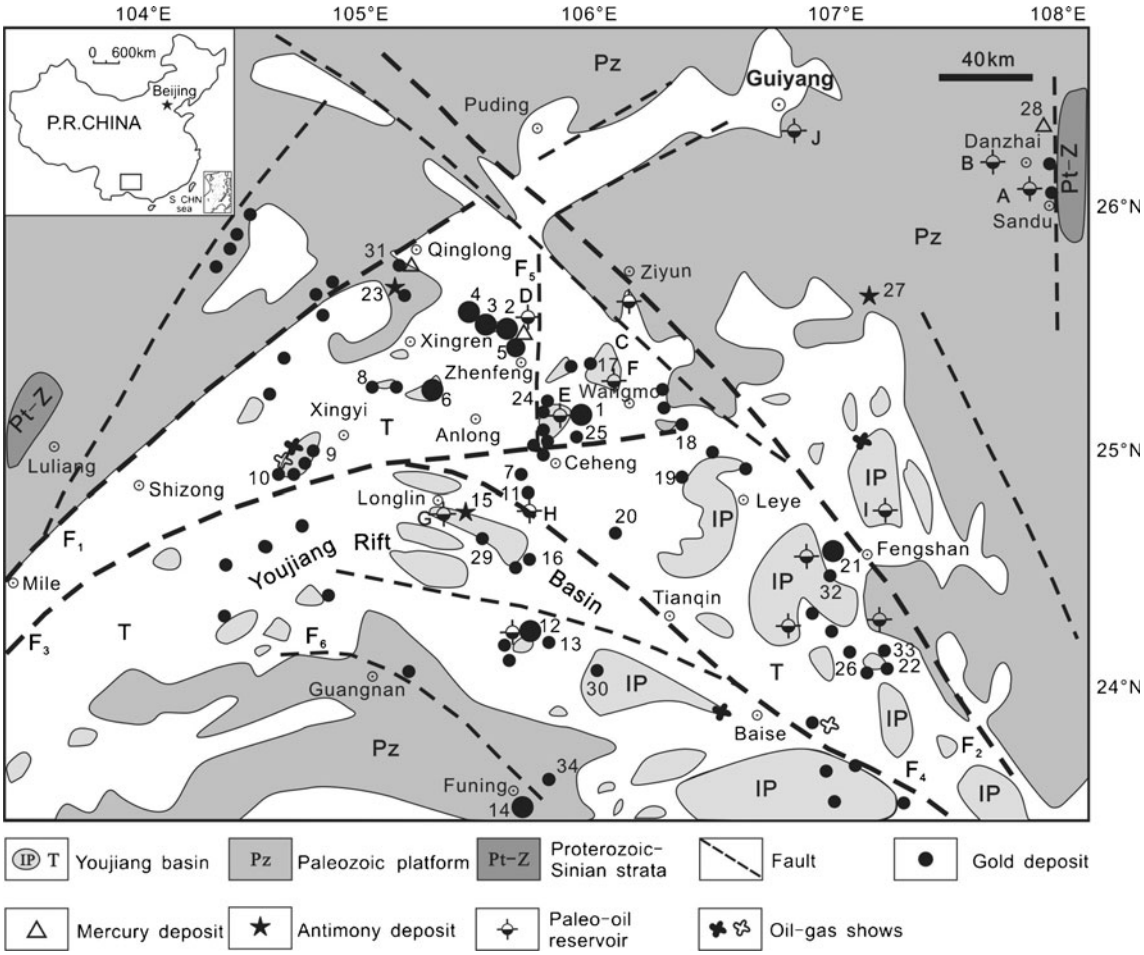

Fig. 1 Simplified geologic map showing distribution of major Au, Sb, and Hg deposits and paleo-reservoirs in the Youjiang basin, South China (modified after Hu et al. 2002; Liu et al. 2002; Wang et al. 2002; Peters et al. 2007; Gu et al. 2010). Faults: F_1 Mile–Shizong fault; F_2 Shuicheng–Ziyun–Bama fault; F_3 Nanpanjiang fault; F_4 Youjiang fault; F_5 Puding–Ceyang fault; F_6 Guangnan–Funing fault. Metal deposits: *1* Lannigou; *2* Shuiyindong; *3* Taipingdong; *4* Zimudang; *5* Bojitian; *6* Getang; *7* Yata; *8* Nibao; *9* Xiongwu; *10* Lubuge; *11* Banqi; *12* Gaolong; *13* Badu; *14* Gedang; *15* Maxiong; *16* Longhuo; *17* Nage; *18* Lekang; *19* Langjin; *20* Baidi; *21* Jinya; *22* Linbu; *23* Dachang; *24* Xingzhai; *25* Linlou; *26* Mingshan; *27* Dushan; *28* Danzhai; *29* Zhe'ai; *30* Sijia; *31* Sixiangchang; *32* Lingyun; *33* Longtian; *34* Jinba. Paleo-oil reservoirs: *A* Danzhai; *B* Majiang; *C* Shitouzhai; *D* Baiceng; *E* Laizishan; *F* Balai; *G* Anran; *H* Banjie; *I* Dachang. *IP* Intrabasinal platform; *T* Triassic strata

basin on a passive continental margin (early Devonian to early Permian), back-arc rift basin (late Permian to middle Triassic), and foreland basin (late Triassic), in response to the opening, northward subduction and closure of the Paleo-Tethys ocean situated to the south of the Yangtze craton (Zeng 1993; Zeng et al. 1995).

In the Devonian, the southwest margin of the Yangtze craton underwent extensional faulting, resulting in formation of the Youjiang rift basin. Sedimentation in the basin during the Devonian to middle Triassic was controlled by a series of NW- and NE-trending extensional faults (syndepositional faults). The topography of the basin was characterized by a complex graben-and-horst (subbasin and platform) style. The boundaries between the subbasins and platforms are marked by syndepositional normal faults. Shallow water limestone and biohermal limestone deposited on the submarine horsts (platforms), while deep water mudstone, siltstone, micrite, chert, and locally, tuffaceous argillite dominated in the grabens (subbasins; Liu et al. 2002; Peters et al. 2007). In the late Triassic, the Youjiang basin evolved into a foreland basin in response to the uplift of the south and southwest margins. A thick sequence of sandstone/mudstone turbidite accumulated on the Devonian to middle Triassic sedimentary rocks. The Indosinian orogeny in the latest Triassic and the subsequent Yanshanian orogeny during the Jurassic to Cretaceous resulted in uplift and folding of the Youjiang basin (Zeng 1993; Zeng et al. 1995; Hu et al. 2002; Liu et al. 2002).

Sedimentary rock hosted disseminated gold deposits in the Youjiang basin have many features in common with the well-known Carlin-type deposits in western USA (e.g., Radtke 1985; Arehart 1996; Hofstra and Cline 2000; Cline

2001; Cline et al. 2005). In general, the gold deposits occur either in the Permian to Triassic carbonate/siliciclastic rocks near the basinal margin, or in and around the intrabasinal, isolated carbonate platforms (horsts) or reefs (Fig. 1). They are more common near the transitional zone between carbonate and siliceous clastic rocks (Yao 1990; Peters et al. 2007). The ore bodies are typically controlled by short-axial anticlines (domes) and associated fracture zones (e.g., the Zimudang, Shuiyindong, and Jinya gold deposits; Fig. 2a), high angle faults (e.g., the Lannigou, Zimudang, and Yata gold deposits; Fig. 2b), and paleo-karst planes or unconformity surfaces (e.g., the Gedang, Getang, Banqi, and Gaolong gold deposits; Fig. 2c, d). The immediate host rocks commonly are impure limestone and mixtures of carbonate and siliceous clastic rocks and locally contain interbedded tuff or volcanoclastic rocks. They typically contain high contents of organic carbon (up to 5 wt%; Lin and Liu 1995) to give the rocks a black to dark gray color (Fig. 3b, c). Hydrothermal alteration mainly consists of silicification, argillization, and decarbonatization. The ore minerals include pyrite, arsenian pyrite, marcasite, arseno-pyrite, realgar, orpiment, stibnite, and cinnabar. Minor base

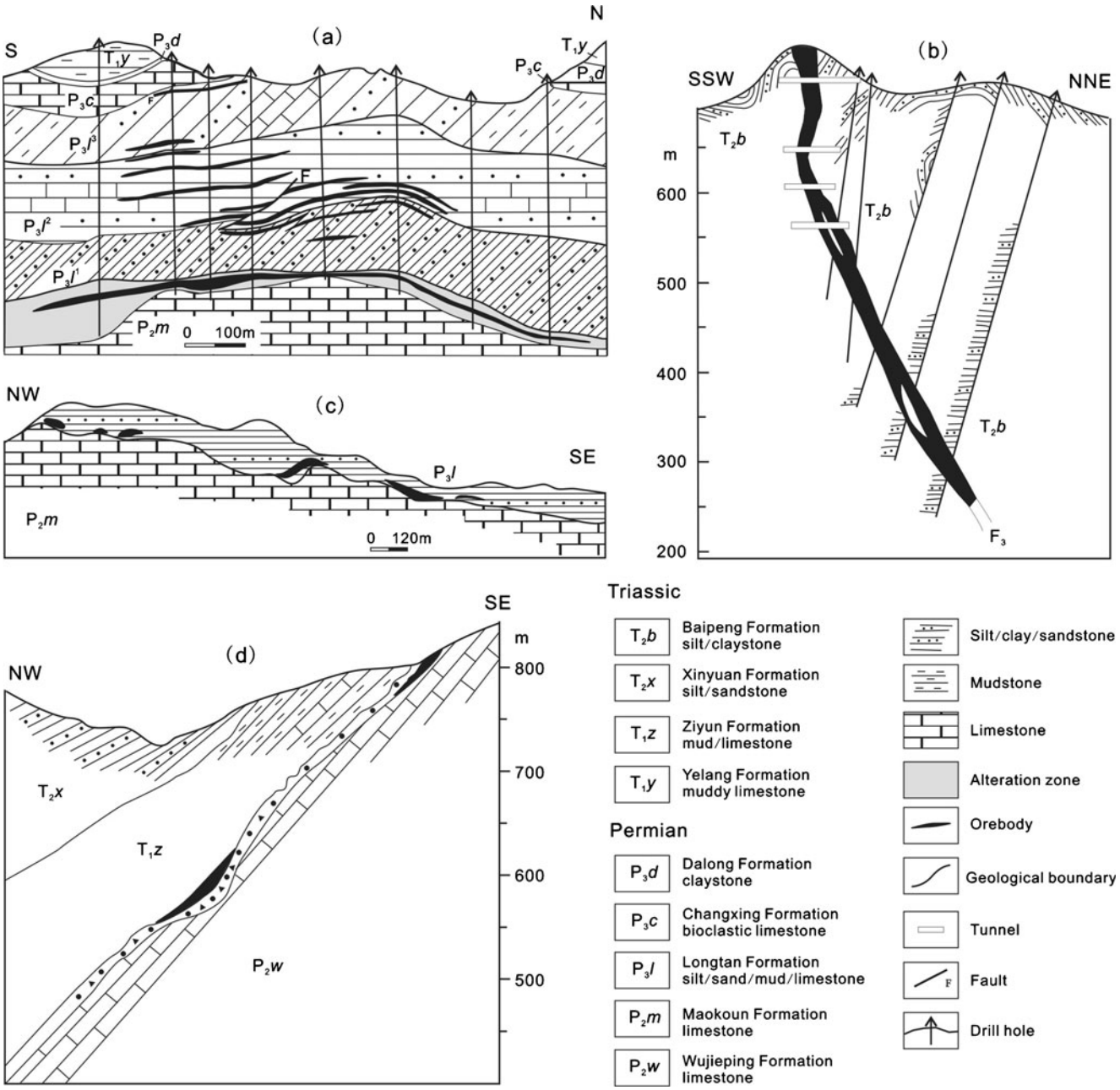

Fig. 2 Cross-sections showing mineralization of typical Carlin-type gold deposits in the Youjiang basin. **a** Shuiyindong deposit (after Liu and Liu 2005). **b** Lannigou deposit (after Luo 1994). **c** Getang deposit (modified after Tao 1990). **d** Banqi deposit (modified after Chen 1986)

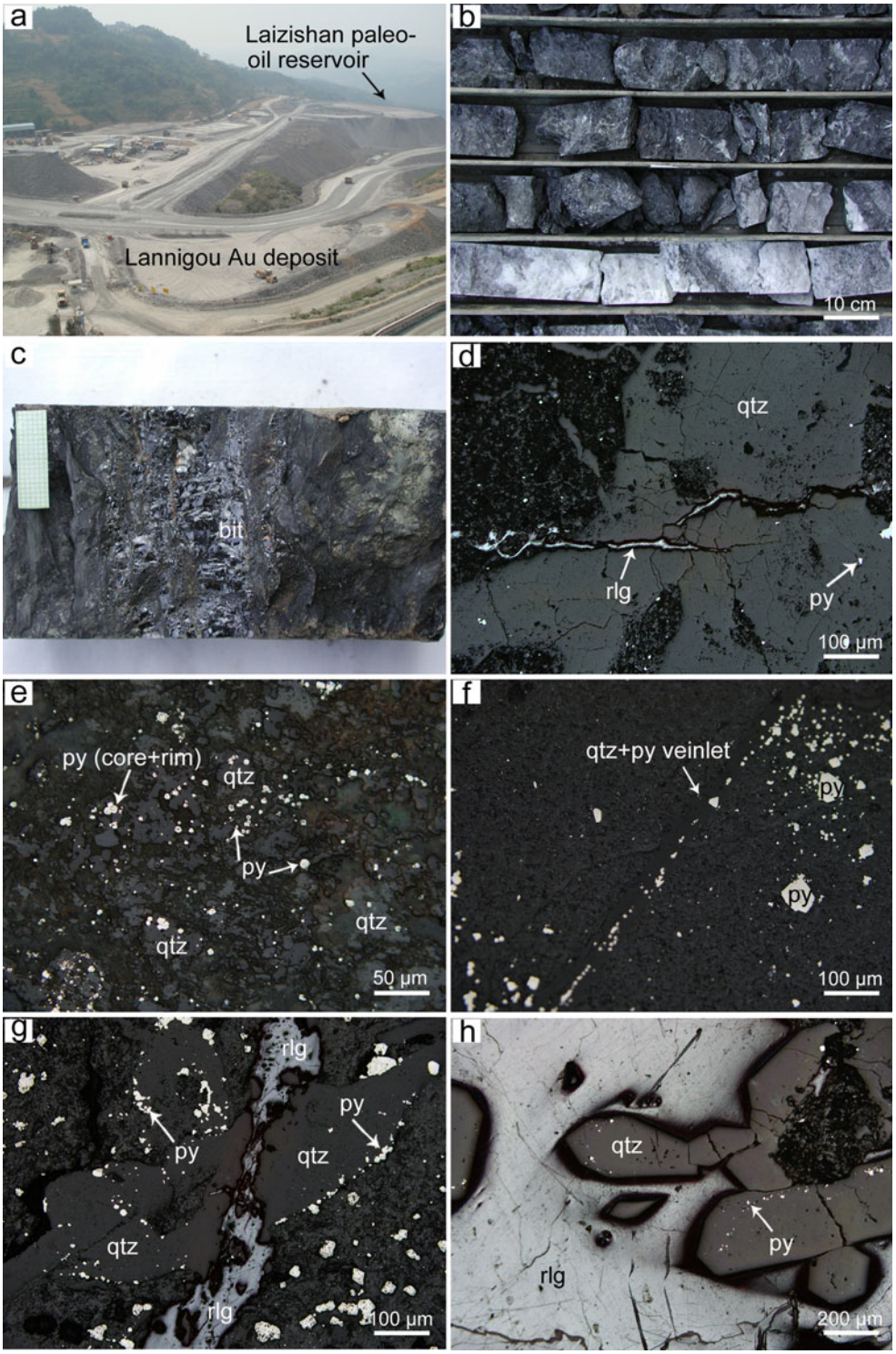

Fig. 3 **a** Photograph showing that the Lannigou gold deposit is spatially close to and only 700 m northeastward away from the Laizishan paleo-oil reservoir. **b** Gold ore hosted in black to dark gray, organic matter-rich siltstone and shale in the Shuiyindong gold deposit. **c** Bitumen veins in gold ore of the Shuiyindong gold deposit. Millimeter paper for scale. **d** Photomicrograph showing early stage milky quartz crosscut by late-stage realgar at the Yata gold deposit. **e** Main stage arsenian pyrite disseminated in a high grade ore sample (Au>100 ppm) from the Shuiyindong gold deposit. The arsenian pyrite typically occurs as tiny anhedral to subhedral grains that are enclosed in or closely associated with pervasive or patchy jasperoidal quartz. Some pyrite grains consist of a Au- and As-poor core and a Au- and As-rich rim. **f** Main stage quartz-pyrite veinlet in the Zimudang gold ore. **g** Photomicrograph showing the main stage quartz-pyrite veinlet crosscut by the late-stage realgar at the Taipingdong gold deposit. **h** Late-stage euhedral quartz crystals overgrown by realgar at the Yata gold deposit. Note the growth zones of quartz crystals delineated by tiny, euhedral to subhedral pyrite grains. Photographs **d**–**h** were taken under reflected plane-polarized light. *bit* Bitumen; *py* pyrite; *rlg* realgar, *qtz* quartz, *cal* calcite

metal sulfides, such as galena, sphalerite, chalcopyrite, and Pb–Sb–As–sulphosalts are also present. Gangue minerals comprise mostly calcite, dolomite, quartz, and illite. Gold is commonly in arsenian pyrite and arsenopyrite, occurring mainly as invisible nanometer-sized sub-microscopic inclusions and subordinately as invisible lattice gold and visible micrometer-sized native gold (Liu et al. 1994, 2002; Hu et al. 2002; Peters et al. 2007). A general lack of igneous rocks near the gold deposits suggests that the ores are not related to magmatism.

The Devonian to Triassic sedimentary rocks in the Youjiang basin contain several suites of petroleum source-reservoir-cap assemblages, in which the deep water facies, organic-rich black mudrock, and carbonaceous limestone

acted normally as hydrocarbon source rocks, while the shallow water facies, platform, and reef carbonate acted as reservoir rocks and the interbedded mudrock/argillaceous siltstone and limestone as cap rocks. Although limited oil exploration drilling in the Youjiang basin to date have only encountered noncommercial gas (methane) shows, exposures of paleo-petroleum reservoirs with abundant solid bitumen as degraded residues of mobile hydrocarbons are widespread in the basin. In general, the paleo-petroleum reservoirs are restricted to the same tectonic units with, and close to, the sedimentary rock hosted Au, Sb, Hg, and As deposits (Figs. 1 and 3a). They occur commonly in carbonate rocks near the basinal margins and in isolated platform and/or reef limestones, especially in the Permian reefs. Bitumens in the paleo-reservoirs have a high thermal maturity, with the reflectance under oil immersion (R_o) of 2.2–4.3% and the H/C ratio of 0.2–0.5, and are interpreted to represent the cracking residue of crude oil (Zhao et al. 2007).

Analytical methods

Our paragenetic study was based on field observations as well as on hand specimens and transmitted and reflected light petrography. Samples used to study the nature of reservoir- and ore-forming fluids include diagenetic cements and vein minerals from the paleo-oil reservoir rocks in Permian reefs, as well as hydrothermal minerals from the Carlin-type gold deposits. Microthermometric studies of fluid inclusions were carried out at the State Key Laboratory (SKL) of Geological Processes and Mineral Resources, China University of Geosciences (Beijing) and the State Key Laboratory of Ore Deposit Geochemistry (SKL-ODG), Institute of Geochemistry (Guiyang), Chinese Academy of Sciences, following the procedures outlined by Shepherd et al. (1985). The phase transitions of fluid inclusions were observed at temperatures from −193 to 600°C using a Linkham THMSG-600 heating/freezing stage. The results are given with an accuracy of ±0.1°C at −22°C and ±2°C at 400°C, relative to standard material. Salinity expressed as weigth percent NaCl eq. was calculated from microthermometric data using the equations of Bodnar (1993). Volatile and hydrocarbon species (e.g., CO_2, N_2, CH_4, and C_2H_6) in individual fluid inclusions were analyzed using a Renishaw Invia reflex-type confocal laser raman microspectrometer (LRM) at the SKL-ODG, following the method described by Burke (2001).

Sm–Nd isotopic ratio measurements were made on an IsoProbe T thermal ionization mass spectrometer at the Analytical Center of Beijing Research Institute of Uranium Geology, following the methods described by Johansson and Kullerud (1993). Nd isotopic ratios were corrected for mass fractionation using a $^{146}Nd/^{144}Nd$ value of 0.7219. Repeated measurements of SHINESTU Nd standard on this mass spectrometer yield a mean $^{143}Nd/^{144}Nd$ ratio of 0.512118±3 (2σ; standard value, 0.512110).

Results

Paragenesis of hydrothermal minerals and organic matter

Integrated petrographic studies on textures, crosscutting relationships, and mineral assemblages of the sedimentary rock hosted gold deposits in the Youjiang basin indicate that most of the deposits exhibit an early stage of quartz± pyrite (stage I), a main stage of auriferous quartz+arsenian pyrite+arsenopyrite+marcasite (stage II), and a late stage of quartz+calcite+realgar±orpiment±native arsenic±stibnite±cinnabar±dolomite (stage III).

The early stage quartz occurs most commonly as milky white veins occasionally containing minor pyrite that is relatively coarse, anhedral to euhedral, and, under the microscope, exhibits high relief and a smooth polish. Both vein quartz and pyrite are locally fractured and cemented or crosscut by the main and late-stage minerals, including quartz, realgar, auriferous arsenian pyrite, and arsenopyrite (Fig. 3d). Electron microprobe analyses (EMPA) indicate that the early stage coarse pyrite is commonly Au and As poor, with gold contents ranging from below to just above detection limits (500 ppm) and arsenic concentrations typically <5 wt% (Fu et al. 2004).

The main stage assemblage consists of gold-bearing arsenian pyrite, arsenopyrite, and marcasite that are most commonly enclosed in pervasive or patchy jasperoidal quartz and, less commonly, disseminated in quartz veins and veinlets in the ore (Fig. 3e, f). Arsenian pyrite and marcasite typically occur as tiny, anhedral to subhedral grains, commonly <10 μm in diameter, whereas arsenopyrite typically occurs as tiny acicular to prismatic crystals surrounding pyrite grains. Arsenian pyrite also commonly forms rims, generally <2 μm thick, around gold-free pyrite cores (Fig. 3e). Under the microscope, arsenian pyrite and marcasite grains have relatively low relief and a poor polish.

Arsenian pyrite and arsenopyrite are the dominant gold-bearing sulfides, in which gold is predominantly invisible and rarely occurs as free native gold grains enclosed in arsenian pyrite, ranging from 0.1 to 6 μm in diameter (Su et al. 2008, 2009a). EMPA showed that gold in arsenian pyrite and arsenopyrite in the Shuiyindong gold deposit ranges from 600 to 3,800 ppm (Su et al. 2008) and from 300 to 1,500 ppm (Zhang et al. 2008), respectively. Arsenic concentrations in the gold-bearing pyrite ranged from 3.37 to 14.06 wt% (Su et al. 2008). At the Yata gold deposit, EMPA showed that arsenian pyrite has an average gold

content of 540 ppm and arsenic content of 10.73% (Ye et al. 1994).

The late-stage quartz, calcite, realgar, and minor orpiment, stibnite, native arsenic, and cinnabar commonly fill open spaces created by fracturing and limestone dissolution and, locally, crosscut and/or enclose stages I and II mineral assemblages (Fig. 3g, h). Trace amounts of sphalerite, galena, and chalcopyrite are occasionally also observed. Open space-filling quartz is characterized by euhedral crystals typically concentrated on the walls of fractures and pores and subsequently overgrown by calcite and realgar. In rare instances, growth zones of the fine euhedral quartz crystals are delineated by the presence of tiny (commonly <5 μm in diameter), euhedral to subhedral pyrite grains (Fig. 3h), possibly indicating that some gold mineralization may have continued to the early phase of stage III. Calcite and realgar are generally free of iron sulfide grains, although rare gold-bearing earlier stage pyrite and/or marcasite grains are locally enclosed by realgar. In the open space-filling assemblage, minor to trace amounts of orpiment, stibnite, native arsenic, and cinnabar are intergrown with or encompassed by realgar.

According to paragenetic and textural relationships based on organic petrology, two principal types of organic matter are present in the gold deposits: In situ alginite disseminated in host sedimentary rocks and hydrothermally migrated bitumen/pyrobitumen disseminated in mineralized rocks and/or occurring as open-space filling in hydrothermal veins and veinlets. Autochthonous alginite appears as lamellae or bands always parallel to bedding planes (Fig. 4a) and is gray, devoid of internal reflections, and isotropic to slightly anisotropic under reflected white light. It typically occurs throughout the host sedimentary rocks and is interpreted to represent algal residues that have been thermally degraded in situ and not subjected to secondary migration (e.g., Glikson et al. 2000).

In most cases, bitumen is so finely dispersed throughout the gold ore that it is normally not macroscopically discernible. Microscopically, bitumen appears as discrete, angular to subspherical grains and, under reflected white light, is brownish gray, isotropic to weakly anisotropic, and of slightly higher reflectance compared to the alginite residue. It occurs commonly in mineralized host rocks, is particularly prevalent in proximal zones of high grade ores, and occurs less commonly as open-space filling in hydrothermal veins and veinlets, but is absent in barren sedimentary rocks. In general, bitumen dispersed in mineralized rocks is intimately associated and/or intergrown with the main stage jasperoidal quartz patches, arsenian pyrite, and arsenopyrite (Fig. 4b, c). Most commonly, bitumen in veins and veinlets is paragenetically associated with stages II and III mineral assemblages (Fig. 4d–h), occurring either as discrete grains disseminated in vein quartz containing arsenian pyrite and arsenopyrite (stage II) or, more commonly, along with quartz, calcite, realgar, stibnite, and/or orpiment in veins of stage III. In rare cases, bitumen occurs also in the early stage quartz veins.

Macroscopically, bitumen in the paleo-petroleum reservoirs in the Youjiang basin is most commonly observed in open spaces created by limestone dissolution and/or faulting and occurs either alone or associated with calcite (Fig. 5a–c). Less commonly, bitumen also occurs as thin films along stylolites in carbonate rocks (Fig. 5d). Where bitumen occurs together with calcite, it is typically concentrated along pore/vein centers as well as along the wall of pores and fractures (Fig. 5b, c, e, and f), indicating approximately coeval precipitation. At the microscopic scale, solid inclusions of bitumen, ranging from <1 μm up to 1–2 mm in diameter, are abundant in pore- and fissure-filling calcite adjacent to the contact with coeval massive bitumen but diminish with distance from this contact (Fig. 5g). These solid inclusions of bitumen typically exhibit a spheroidal shape and spatially are associated with fluid inclusions of both hydrocarbons and aqueous phases (Fig. 5h).

Fluid inclusion petrography

Fluid inclusions in hydrothermal quartz and calcite from the Carlin-type gold deposits in the Youjiang basin are relatively abundant and large, varying in size from 5 to 60 μm and typically from 10 to 30 μm. They have a variety of shapes, including negative crystal, rounded, elongate, square, rhombic, and less commonly, needle-like or irregular forms. The majority of the fluid inclusions appear to be primary, occurring along growth zones of quartz and calcite with negative crystal shapes, or as isolated inclusions randomly scattered in host minerals. Secondary fluid inclusions occurring along microfissures with oblate or irregular shapes are also observed.

Five types of fluid inclusions have been identified based on their phase contents at room temperature. Type I inclusions are mono-phase liquid (Ia) or two-phase liquid-rich (Ib) H_2O inclusions with a vapor bubble of 5–20 vol% of the whole inclusion (Fig. 6a). They are the most abundant inclusions in minerals of all hydrothermal stages. Type II inclusions are mono-phase vapor (IIa) or two-phase (liquid+vapor) vapor-rich (IIb) CO_2 inclusions with proportions of a vapor CO_2 phase ranging from 50 to 90 vol% (Fig. 6b, c). They occur more commonly in the late-stage quartz and calcite associated with realgar, orpiment, and stibnite than in the main stage quartz veinlets with arsenian pyrite and arsenopyrite, but are rare or absent in the early stage milky quartz veins. Type III inclusions are three-phase CO_2–H_2O inclusions consisting of liquid plus vapor CO_2 and liquid H_2O (Fig. 6d, e). The volume of liquid plus

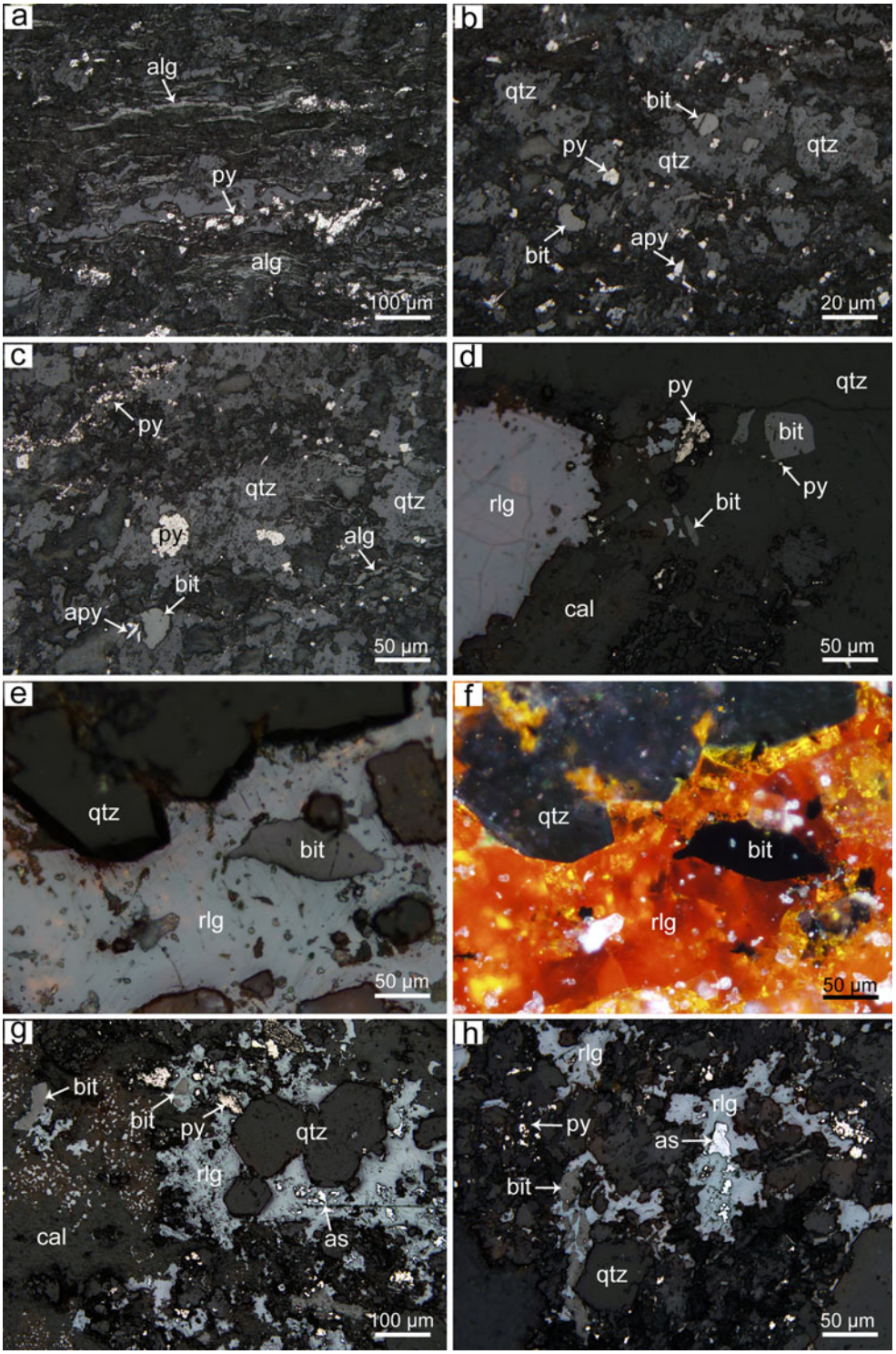

Fig. 4 Photomicrographs showing organic matter and its paragenetic relationships to hydrothermal minerals in the gold deposits. **a** Autochthonous alginite appears as lamellae or bands parallel to bedding planes of the host sedimentary rock (calcareous siltstone) at Taipingdong. **b**, **c** Angular to subspherical, disseminated bitumen is intimately associated with main stage jasperoidal quartz patches, arsenian pyrite, and arsenopyrite in the gold ore at Shuiyindong. Bitumen is distinguished from autochthonous alginite by its form and relatively higher reflectance. **d** Bitumen disseminated in the main stage quartz-pyrite vein in the gold ore from Taipingdong. Late-stage calcite and realgar filled open spaces of the ore. **e**, **f** Late-stage euhedral quartz crystals overgrown by realgar containing bitumen in the Taipingdong gold ore. **g**, **h** Late-stage quartz, calcite, native arsenic, and bitumen fill the open spaces created by fracturing at Taipingdong. Photographs were taken under reflected plane-polarized light except for **f**, which was under reflected crossed-polarized light. *alg* Alginite; *bit* bitumen, *py* pyrite; *apy* arsenopyrite; *rlg* realgar; *as* native arsenic; *qtz* quartz; *cal* calcite

vapor CO_2 is highly variable, ranging from 5% up to 95% of the inclusions. Fluid inclusions of type III are commonly observed both in the main stage quartz veinlets and in the late-stage drusy quartz and calcite.

Type IV inclusions are mono-phase vapor hydrocarbon (CH_4) inclusions (Fig. 6c, f). In rare cases, the vapor hydrocarbon inclusions contain a thin (<2 μm thick), light brown rim of liquid oil around the inclusion walls (Fig. 6g), probably indicating that the vapor hydrocarbon partially condensed into liquid oil in response to the decrease in pressure and temperature after its trapping. Type V inclusions are two-phase CH_4–H_2O inclusions consisting of a vapor hydrocarbon phase (ranging from 40% to 95% by volume) and an aqueous liquid phase (Fig. 6h, i). Fluid inclusions of

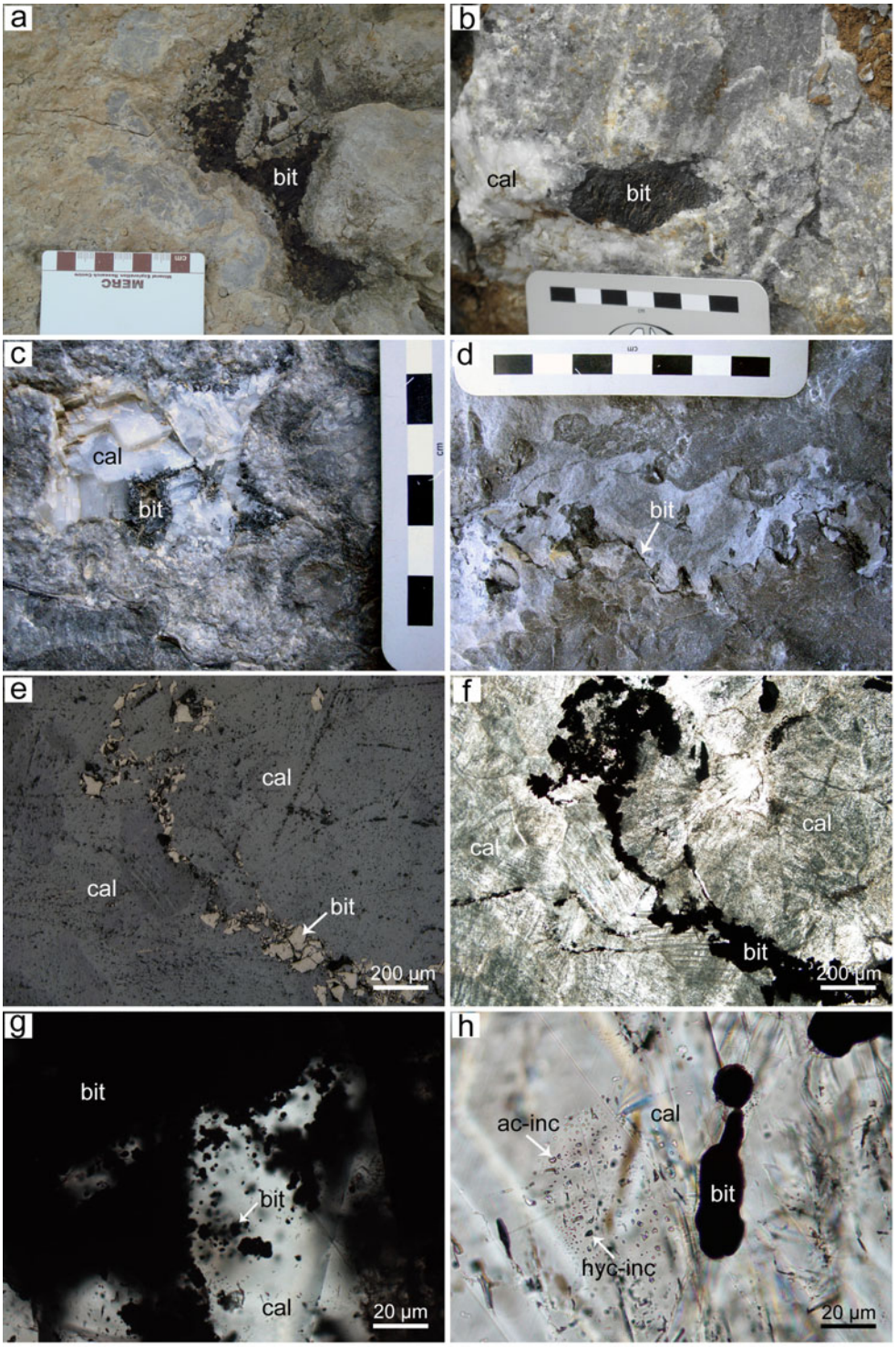

Fig. 5 Photographs showing bitumens in Permian paleo-oil reservoirs in the Youjiang basin. **a** Pore- and fissure-filling bitumen in the bioclastic limestone reservoir at Laizishan. **b** Bitumen occurs in the center of calcite vein in the Baiceng limestone reservoir. **c** Open space-filling calcite with bitumen concentrated along the wall and at the center of the pore in the Banjie limestone reservoir. **d** Bitumen occurs as thin films along stylolites in the reservoir rock at Banjie. **e**, **f** Photomicrographs showing bitumen concentrated along the center of calcite vein in the Pingrao limestone reservoir. **g** Photomicrograph of pore-filling bitumen and calcite at Banjie. Spheroidal bitumens occur as solid inclusions in pore-filling calcite adjacent to the contact with coeval massive bitumen but diminish with distance from this contact. **h** Spheroidal solid bitumen inclusions are associated with hydrocarbon and aqueous fluid inclusions in the pore-filling calcite near the contact with massive bitumen at Pingrao. Photomicrograph **e** was taken under reflected plane-polarized light; photomicrographs **f**–**h** were taken under transmitted plane-polarized light. *bit* Bitumen; *cal* calcite; *hyc-inc* hydrocarbon (vapor CH_4) inclusion; *aq-inc* aqueous inclusion

types IV and V occur commonly in quartz and calcite of the main and late stages, although they are occasionally also observed in the early stage milky quartz. In addition, abundant solid bitumens are also observed in the main and late-stage quartz and calcite (rare in the early stage milky quartz), occurring either as discrete inclusions or as a solid phase within aqueous fluid inclusions (Fig. 6a, g).

Fluid inclusions in calcite occurring as diagenetic cements or calcite veins from the paleo-oil reservoirs of Permian reefs vary in size from <3 up to 45 μm, with a large population around 5–15 μm. Most of the inclusions are of primary origin and occur in clusters or scatters with a negative (typically rhombic) crystal shape. Secondary fluid inclusions occur along microfissures with elongate, needle-like, or irregular

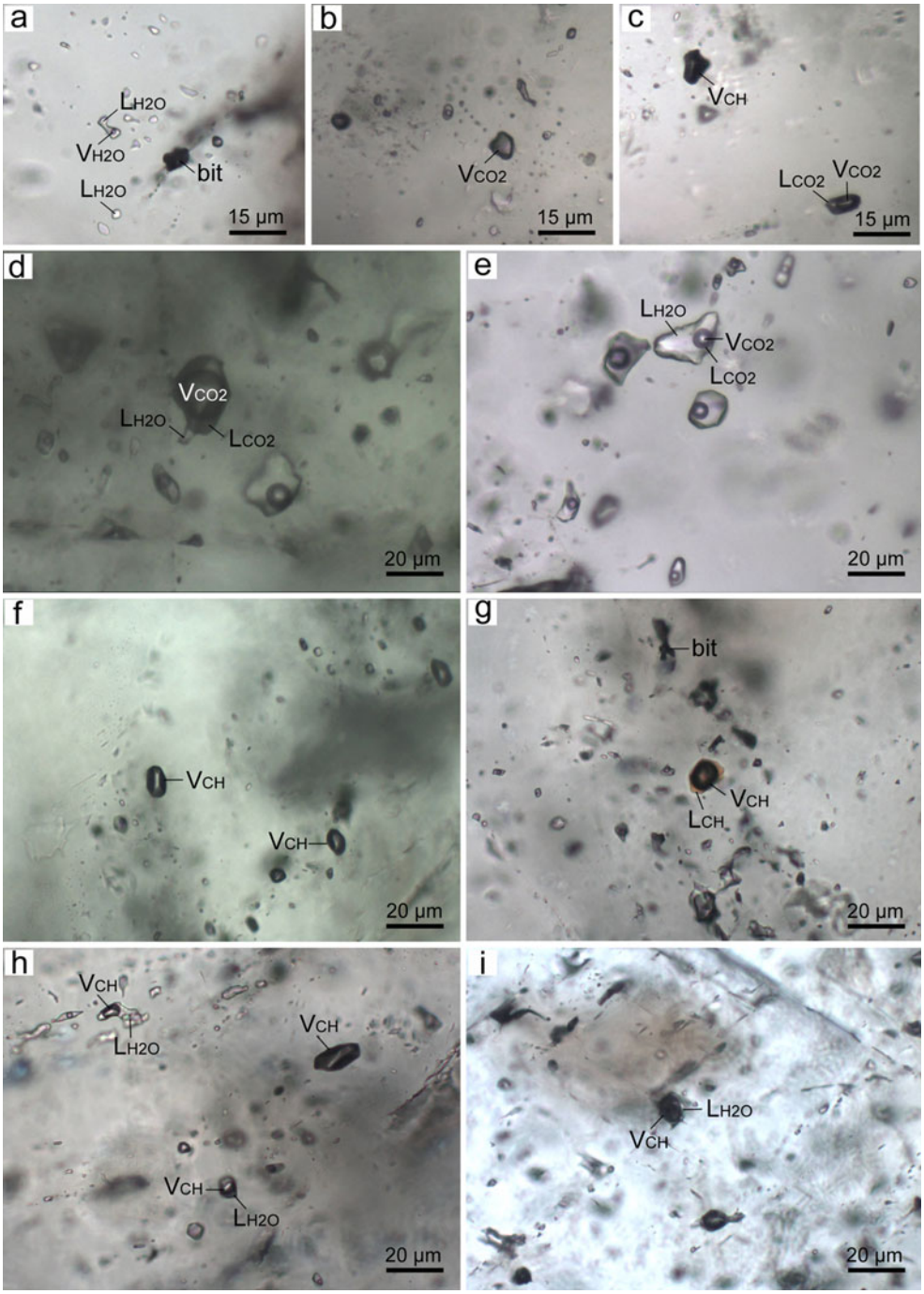

Fig. 6 Photomicrographs of fluid inclusions in the gold deposits. **a** Primary type I aqueous inclusions in late-stage drusy quartz from the Yata deposit. Note the solid bitumen inclusion in a healed microfissure. **b** Mono-phase vapor CO_2 inclusions (type IIa) in the main stage quartz at Shuiyindong. **c** Two-phase, vapor-rich CO_2 inclusions (type IIb) and mono-phase vapor hydrocarbon (CH_4) inclusions (type IV) in the main stage quartz from Shuiyindong. **d**, **e** Three-phase CO_2–H_2O inclusions (type III) have highly variable volumes of liquid plus vapor CO_2 and are intergrown with type I aqueous inclusions in the main stage quartz at Shuiyindong. **f** Primary, mono-phase vapor hydrocarbon (CH_4) inclusions (type IV) in the late-stage drusy quartz from the Taipingdong deposit. **g** The vapor hydrocarbon inclusion of type IV in the late-stage drusy quartz at Taipingdong contains a thin, light brown rim of liquid oil around the inclusion wall. Note also the presence of solid bitumen inclusions. **h** Coexistence of two-phase CH_4–H_2O inclusions (type V), type IV vapor CH_4 inclusions, and type I aqueous inclusions in the late-stage drusy quartz at Taipingdong. **i** Type V two-phase CH_4-H_2O inclusions in the late-stage calcite from Zimudang. L_{H_2O} liquid H_2O; V_{H_2O} vapor H_2O; L_{CO_2} liquid CO_2; V_{CO_2} vapor CO_2, L_{CH} liquid hydrocarbon; V_{CH} vapor hydrocarbon (CH_4)

shapes. Except for the common occurrence of mono-phase liquid hydrocarbon (C_2H_6) inclusions in paleo-oil reservoirs (Fig. 7a), fluid inclusion types are comparable with those occurring in the gold deposits described above.

In general, three generations of pore- and fissure-filling calcite with different fluid inclusion assemblages are recognized (Gu et al. 2007b). The early diagenetic calcite (I), occurring either as intergranular cements or as overgrowths on detrital grains, predominantly contains mono-phase liquid and two-phase liquid-rich H_2O inclusions, though liquid hydrocarbon (C_2H_6) inclusions are occasionally observed. In the late diagenetic pore- and fissure-filling calcite (II) associated with bitumen, the liquid hydrocarbon (C_2H_6), mono-phase vapor CH_4, two-phase CH_4–H_2O, and two-phase liquid-rich H_2O inclusions are dominant (Fig. 7b, d, e, and f). In the late diagenetic calcite (III)-bitumen veins crosscutting both calcite-I and calcite-II, fluid inclusions are dominated by mono-phase vapor CH_4 (Fig. 7c). The calcite-II and calcite-III are thus interpreted to have precipitated during the peak oil- and gas-generation stage (Gu et al. 2007b).

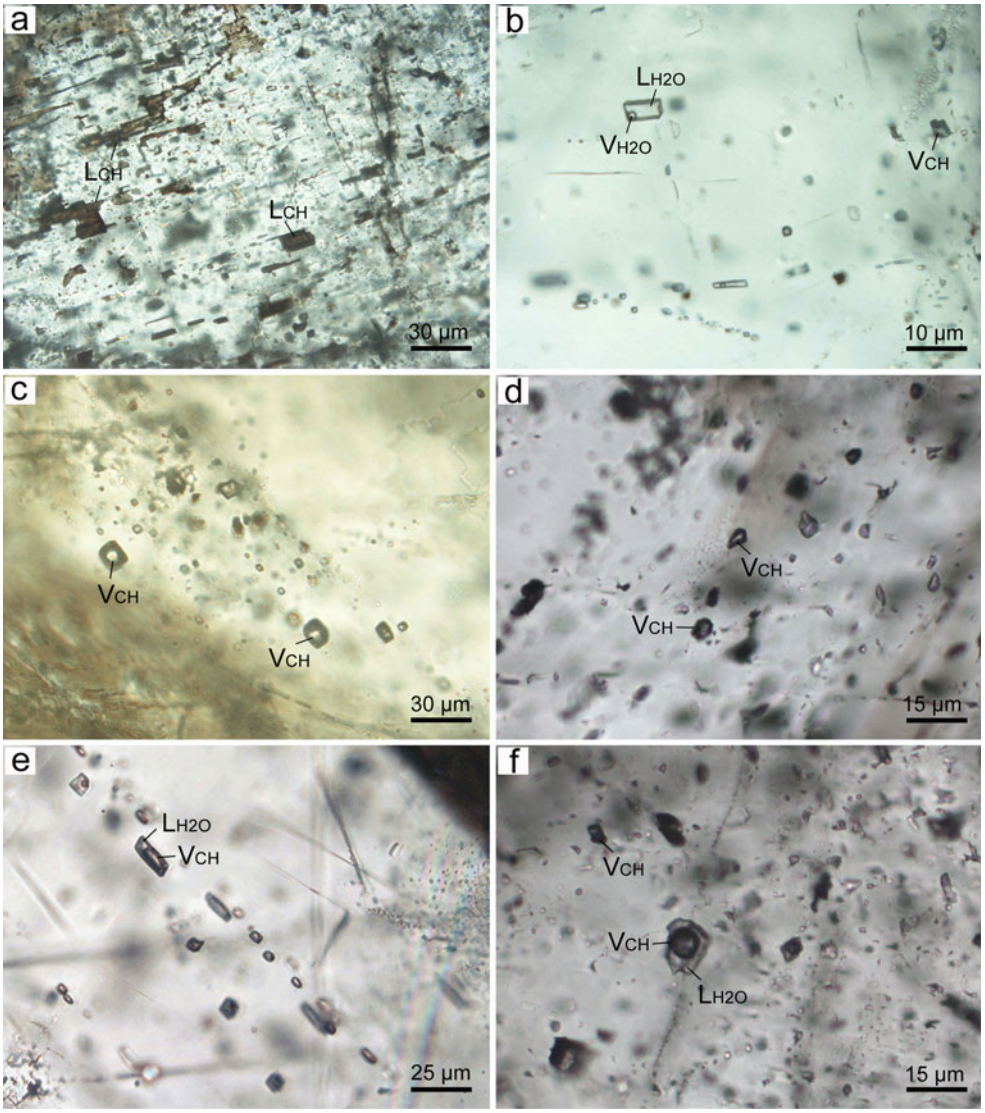

Fig. 7 Photomicrographs of fluid inclusions in the paleo-oil reservoirs. **a** Liquid hydrocarbon (C_2H_6) inclusions in the late diagenetic calcite from Shitouzhai. **b** Aqueous inclusions and mono-phase vapor CH_4 inclusions in the late diagenetic calcite at Shitouzhai. **c** Vapor hydrocarbon (CH_4) inclusions along the growth zone of late diagenetic calcite from Laizishan. **d** Vapor hydrocarbon (CH_4) inclusions and aqueous inclusions in the late diagenetic calcite at Banjie. **e** Two-phase CH_4–H_2O inclusions along the growth zone of late diagenetic calcite from Shitouzhai. **f** Coexistence of two-phase CH_4–H_2O inclusions and vapor CH_4 inclusions in the late diagenetic calcite from Banjie. L_{H_2O} Liquid H_2O, V_{H_2O} vapor H_2O, L_{CH} liquid hydrocarbon (C_2H_6), V_{CH} vapor hydrocarbon (CH_4)

Homogenization temperature and salinity

Thermometric analyses were performed principally on the primary two-phase aqueous inclusions (type I), which were relatively large (>7 μm) and preferably rounded and polygonal. Two common thermometric procedures, heating and freezing, were employed to determine the homogenization temperature and melting temperature, respectively. The two-phase (liquid+vapor) aqueous inclusions are dominated by a liquid phase and homogenized into the liquid phase during heating.

Fluid inclusions in the early stage milky quartz (stage I) from the Carlin-type gold deposits have a homogenization temperature range of 201–390°C (typically 230–270°C) and a salinity range of 2.6 to 7.2 wt% NaCl eq. (Table 1). Homogenization temperatures in the main stage quartz associated with gold mineralization (stage II) range from 170°C to 290°C (typically 200–230°C) with an average of 215°C. The salinity of the main stage ore fluid varies between 1.9 and 8.7 wt% NaCl eq. with a mode around 5.3 wt % NaCl eq. Fluid inclusions in the late-stage drusy quartz and calcite (stage III) have homogenization temperatures ranging from 85°C to 231°C (typically 120–160°C, average 145°C) and a salinity range of 0.2 to 7.9 wt% NaCl eq. (typically 2.0–5.6 wt% NaCl eq., average 4.0 wt% NaCl eq.).

Homogenization temperatures of the aqueous fluid inclusions in calcite from the Permian paleo-oil reservoirs vary from 73°C to 219°C, mostly from 90°C to 180°C (Table 2). The fluid inclusions in the early diagenetic calcite-I have relatively low homogenization temperatures varying from 73°C to 87°C with an average of 80°C, while those in the late diagenetic calcite-II and calcite-III show wider and higher homogenization temperature ranges of 81–144°C (mostly 90–115°C, average 110°C) and 86–219°C (mostly 110–180°C, average 150°C), respectively. The salinity of the paleo-oil reservoir fluid varies between 0.2 and 19.8 wt% NaCl eq., mostly between 2 and 8 wt% NaCl eq.

Table 1 Summary of aqueous fluid inclusion data for Carlin-type gold deposits in the Youjiang basin

Au deposit	Host mineral/stage	Homogenization temperature (°C)		Salinity (wt% NaCl eq.)		Data source
		Range/number of measurements	Mean	Range/number of measurements	Mean	
Taipingdong	Quartz/I	201–269/49	233	2.6–7.2/38	4.7	This study
	Quartz/II	181–255/67	216	1.9–7.3/57	5.2	
	Calcite/III	97–172/40	123	0.2–5.7/31	2.0	
Shuiyindong	Quartz/I	218–231/14		5.7–6.9/14		Su et al. (2009a)
	Quartz/II	210–240/36	222	2.6–5.7/39	4.9	Xia (2005)
	Calcite/III	126–182/25	150	0.2–1.7/23	0.6	This study
Zimudang	Quartz/II	170–273/83	207	2.1–7.5/88	4.9	
	Calcite/III	95–205/71	148	0.2–5.7/56	3.3	
Bojitian	Calcite/III	117–193/34	155	0.5–6.9/33	4.1	
Lannigou	Quartz/I	240–369/28				Su (2002)
	Quartz/II	183–272/53	219	4.0–8.7/40	6.6	This study
	Quartz/III	93–186/72	130	0.4–7.7/63	4.8	
	Calcite/III	85–187/29	129	0.5–7.7/25	4.2	
Yata	Quartz/I	242–299/12		5.6–6.1		Su (2002)
	Quartz/II	181–235/68		3.4–5.6		
	Quartz/III	106–231/80	165	0.7–7.9/77	5.6	This study
Nage	Quartz/I	241–272/7				Su (2002)
	Quartz/II	181–237/14				
Gedang	Quartz/I	234–390/130				
	Quartz/II	181–253/134				
	Quartz/III	145–176/27				
Badu	Quartz/II	172–235/52				
	Quartz+calcite/III	92–163/23				
Banqi	Quartz/I	310–360				Li et al. (1989)
	Quartz/II	210–290		2.3–4.2/3.2		
	Quartz+calcite/III	110–190				

Laser Raman microspectrometer analysis

In the paleo-oil reservoirs, the vapor hydrocarbon inclusions (type IV-a) and the vapor phase of hydrocarbon-H_2O inclusions (type V) are dominated by CH_4 (73.1–100 mol%) with a small amount of CO_2 (0–26.9 mol%), while the liquid hydrocarbon inclusions (type IV-b) are composed of C_2H_6 (Table 3). In the vapor CO_2 inclusions (type II) and CO_2–H_2O inclusions (type III), CO_2, CH_4, and N_2 account for 30.9–91.1, 7.8–45.5, and 0–44.4 mol%, respectively. In the gold deposits, the vapor hydrocarbon inclusions (type IV-a) are dominated by CH_4 (74.7 mol%), with subordinate CO_2 (23.3 mol%) and N_2 (2.0 mol%). The volatile phases of CO_2–H_2O inclusions (type III) are composed of CO_2 (23.3–100 mol%), CH_4 (0–74.7 mol%), and N_2 (0–17.0 mol%).

Sm–Nd isochron age

Sm–Nd isotopic analyses were performed on the hydrocarbon inclusion-bearing, pore- and fissure-filling calcite-III associated with bitumen in the Shitouzhai Permian reef paleo-oil reservoir in Guizhou province (Table 4). Four samples display a good linear relationship on the $^{147}Sm/^{144}Nd$ vs. $^{143}Nd/^{144}Nd$ diagram (Fig. 8) with a correlation coefficient of 0.9887. These data points provide a Sm–Nd isochron age of 182±21 Ma (2σ) (MSWD=0.026) with an initial $^{143}Nd/^{144}Nd$ ratio of 0.512379±0.000018.

Discussion

Spatial relationship

As described above, the sedimentary rock hosted Au, Sb, Hg, and As deposits in the Youjiang basin are restricted to the same tectonic units as the paleo-oil reservoirs (Fig. 1) and commonly occur in the basinal margin and intrabasinal isolated platforms and/or reefs. The ore deposits are spatially close to the paleo-oil reservoirs. For instance, the Banqi Au deposit is close to the Banjie paleo-reservoir, the Maxiong Sb–Au deposit is adjacent to the Anran paleo-reservoir, the Shuiyindong Au deposit is near the Baiceng

Table 2 Summary of aqueous fluid inclusion data for paleo-oil reservoirs in the Youjiang basin

Paleo-oil reservoir	Diagenetic stage (host mineral)	Homogenization temperature (°C)		Salinity (wt % NaCl eq.)	
		Range/number of measurements	Mean	Range/number of measurements	Mean
Shitouzhai	Early (calcite-I)	74–87/12	80		
	Late (calcite-II)	81–133/34	104	6.7–7.3/2	7.0
	Late (calcite-III)	92–165/31	129	1.6–13.7/8	5.4
Balai	Early (calcite-I)	78–86/6	82		
	Late (calcite-II)	91–111/13	98		
	Late (calcite-III)	126–133/7	129		
Nashui	Early (calcite-I)	73–86/5	80		
	Late (calcite-II)	117–133/6	125		
Laizishan	Late (calcite-II)	92–144/16	121	3.6–5.8/6	4.8
Pingrao	Late (calcite-II)	97–129/12	116	4.6/1	4.6
Nongnaao	Late (calcite-III)	116–195/51	152	2.0–8.8/48	5.8
Baiceng	Late (calcite-III)	93–219/84	170	1.2–19.8/67	9.2
Banjie	Late (calcite-III)	100–196/123	157	0.5–5.9/103	4.2
Yang 1	Late (calcite-III)	86–149/49	115	0.2–4.8/16	2.3
Shuang 1	Late (calcite-III)	100–163/22	139	0.7–4.2/5	1.7
Anran	Late (calcite-III)	91–200/34	136	1.6–10.2/10	7.1

paleo-reservoir, and the Lannigou Au deposit is only 700 m northeast of the Laizishan paleo-reservoir (Fig. 3a; Gu et al. 2007a).

On the deposit scale, gold ore is spatially associated with organic matter. The immediate host rock is characterized by a black to dark gray color with high contents of organic carbon (Fig. 3b, c). Bitumen is common in the gold ore and, in some gold districts, is used by miners as a guide to gold ore. Bitumen in the gold deposits is commonly present in mineralized host rocks, particularly close to high grade ore, but is absent in barren sedimentary rocks. Bitumen dispersed in mineralized rocks is closely associated and/or intergrown with the main stage jasperoidal quartz, arsenian pyrite, and arsenopyrite (Fig. 4b, c). In the main and late-stage quartz and calcite, solid bitumens occurring either as intragranular discrete inclusions or as a solid phase in aqueous fluid inclusions are also observed. These observations strongly suggest an intimate relationship between

Table 3 Laser Raman spectrometry of hydrocarbon and CO_2 phases in fluid inclusions from paleo-oil reservoirs and gold deposits in the Youjiang basin

Paleo-oil reservoir/ Au deposit		Fluid inclusion type/ number of measurements	Molal percentage (mol%)			
			CO_2	N_2	CH_4	C_2H_6
Paleo-oil reservoir	Shitouzhai	Type IV-a/9			100.0	
		Type IV-b/1				100.0
		Type V/6	0.0–16.1		83.9–100.0	
	Laizishan	Type IV-a/2	0.0–10.7		89.3–100.0	
		Type V/1	12.3		87.7	
	Pingrao	Type IV-a/7	0.0–26.9	0–0.5	73.1–100.0	
	Yang 1	Type III/3	73.5–91.1		8.9–26.5	
		Type V/1			100.0	
	Shuang 1	Type II/2	61.3–80.8	4.4–11.4	7.8–34.3	
		Type III/4	30.9–73.1	2.5–44.4	17.9–45.5	
Au deposit	Shuiyindong	Type III/7	75.0–100.0	0.0–9.5	0.0–25.0	
		Type IV-a/1	23.3	2.0	74.7	
	Yata[a]	Type III/15	75.0–97.3	2.7–17.0	0.0–8.0	
	Lannigou[a]	Type III/8	88.8–96.4	3.6–10.8	0.0–6.2	
	Badu[a]	Type III/5	94.6–98.5	1.5–5.4	0.0	

Fluid inclusion type: *II* vapor CO_2 inclusion; *III* CO_2 (liquid+vapor)–H_2O (liquid) inclusion; *IV-a* vapor hydrocarbon inclusion; *IV-b* liquid hydrocarbon inclusion; *V* hydrocarbon (vapor)–H_2O (liquid) inclusion

[a]From Su (2002)

Table 4 Sm–Nd isotopic composition of the calcite-III associated with bitumen from the Shitouzhai paleo-oil reservoir

Sample number	Sm (ppm)	Nd (ppm)	$^{147}Sm/^{144}Nd$	$^{143}Nd/^{144}Nd$	Error (2σ)
ZY19-2	0.401	1.958	0.1238	0.512520	±0.000024
ZY13	0.073	0.399	0.1100	0.512485	±0.000037
ZY15	0.863	3.486	0.1496	0.512559	±0.000015
ZY17-2	0.759	3.359	0.1367	0.512542	±0.000137

bitumen precipitation and gold mineralization. Where bitumen occurs in hydrothermal veins and veinlets, it is paragenetically associated with stages II and III mineral assemblages (Fig. 4d–h), though rare bitumen in the early stage quartz veins is also observed. This further suggests that hydrocarbons were entrained with the hydrothermal fluids throughout the paragenetic sequence.

Hydrocarbon fluid inclusions, ranging from those filled only by vapor hydrocarbons (CH_4, type IV) to inclusions consisting of a vapor hydrocarbon phase (CH_4) and an aqueous liquid phase (type V), are common in quartz and calcite veins/veinlets of stages II and III (Fig. 6f–i) and less common or rare in stage I milky quartz veins. They typically occur together with CO_2 inclusions (type II), CO_2–H_2O inclusions (type III), and aqueous inclusions (type I). Such a paragenetic relationship provides evidence that at least during the main periods of the hydrothermal activity responsible for gold mineralization, the ore fluids consisted of an aqueous solution and an immiscible hydrocarbon phase (e.g., Peabody 1993; Sherlock 2000).

The presence of abundant organic matter in the classical Carlin-type gold deposits in Nevada has been widely documented; however, its role in ore formation has been a subject of debate (e.g., Radtke and Scheiner 1970; Radtke 1985; Ilchik et al. 1986; Leventhal and Hofstra 1990; Presnell 1993; Gu 1996; Hofstra and Cline 2000; Cail and Cline 2001; Gu et al. 2002; Cline et al. 2005). In most deposits, the organic carbon in the ores is either indigenous to the host rock or was introduced as liquid petroleum and subsequently matured or overmatured as solid residue bitumen or pyrobitumen, prior to gold mineralization (e.g., Christensen 1993; Hofstra and Cline 2000). Therefore, organic matter in these deposits is considered to play little or no role in gold precipitation (Hofstra and Cline 2000; Emsbo et al. 2003).

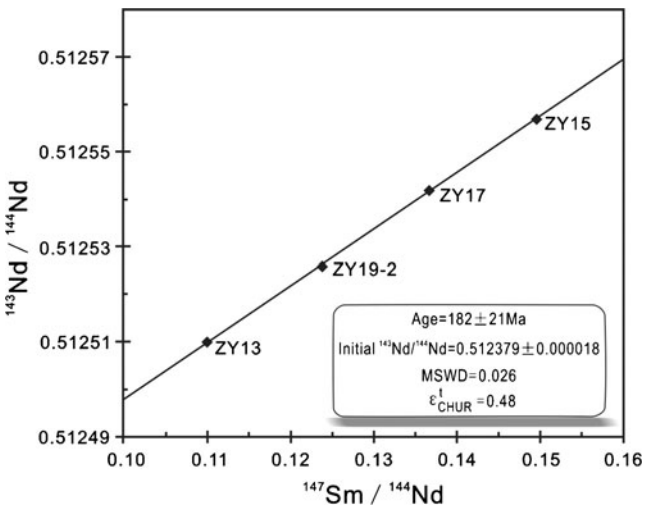

Fig. 8 Sm–Nd isochron of the hydrocarbon inclusion-bearing, pore- and fissure-filling calcite-III associated with bitumen from the Shitouzhai paleo-oil reservoir

In contrast, a close association of hydrocarbons and the Carlin-type gold mineralization was also reported in the Yankee basin in the southern Alligator Ridge mining district, Nevada (Hulen et al. 1994; Hulen and Collister 1999). The Yankee basin Carlin-type gold deposits contain abundant liquid oil in vugs, along fractures, and in fluid inclusions. The fluid inclusion and free oils in the gold orebodies are geochemically equivalent and have similar thermal maturities (early to peak oil-generation stage). Timing of entrapment of the fluid-inclusion oils is paragenetically constrained as dominantly before and during mineralization, while the associated free oils could have arrived before, during, or after mineralization (Hulen and Collister 1999). Hulen and Collister (1999) suggested that the Yankee fluid-inclusion oils were involved in the gold-mineralizing hydrothermal system but were not thermally degraded to pyrobitumen. Nutt and Hofstra (2003) argued, however, that the calcite containing liquid petroleum inclusions at Yankee is post-ore rather than pre- or syn-ore as interpreted by Hulen and Collister (1999).

Temporal relationship

The mineralization age of Carlin-type gold deposits in the Youjiang basin is still in dispute because of the common lack of minerals that are suitable for isotopic dating. A few available data outline a wide range of ages from the late Permian to early Cretaceous. In the Jinya gold deposit, for example, Rb–Sr isotopic dating on the fluid inclusions in auriferous pyrite and arsenopyrite yielded an isochron age of 267±28 Ma, while Au-bearing hydrothermal sericite defined an Rb–Sr isochron age of 206±12 Ma (Wang 1992). In the Lannigou gold deposit, Rb–Sr isotopic dating on the fluid inclusions in ore-stage quartz and calcite yielded an age of 259±27 Ma (Hu et al. 1995), while Re–Os isotopic dating on auriferous arsenian pyrite indicated

an isochron age of 193±13 Ma (Chen et al. 2007). Recent $^{40}Ar/^{39}Ar$ isotopic dating on sericite separated from quartz–calcite–sericite veins that are interpreted to be approximately coeval with gold mineralization at Lannigou defined a plateau date of 194.6±2 Ma (Chen et al. 2009). This $^{40}Ar/^{39}Ar$ plateau age is consistent with the 193±13 Ma Re–Os isochron date for the auriferous arsenian pyrite obtained by the same authors. Su et al. (2009b) analyzed the Sm and Nd concentrations of hydrothermal calcite veins on the periphery of decarbonated zones at the Shuiyindong gold deposit and obtained Sm–Nd isochron dates of 134±3 to 136±3 Ma that are interpreted to be the age of decarbonation and gold deposition.

The wide range of the reported dates using different geochronologic methods has made it difficult to ascertain if a given isotopic date relates to the gold mineralization. The Rb–Sr dating of fluid inclusions in hydrothermal minerals is probably most questionable due to the analytical problems resulting from generally very low Rb and Sr concentrations in the inclusions (e.g., Kesler et al. 2005). Christensen et al. (1995, 1997) employed the Rb–Sr dating of sulfides to constrain the ages of MVT Pb–Zn deposits and stated that samples with $^{87}Rb/^{86}Sr$ ratios <0.25 would likely not produce a meaningful isochron for Phanerozoic deposits. The $^{87}Rb/^{86}Sr$ ratios of fluid inclusions of all nine pyrite and arsenopyrite samples that yielded an age of 267±28 Ma at the Jinya deposit range from 0.079 to 0.174 (Wang 1992), while those of four quartz and calcite samples that formed an age of 259±27 Ma from the Lannigou deposit are highly variable, with two samples <0.25 (0.096–0.228) and the other two >0.25 (0.288–0.758; Hu et al. 1995). Therefore, the Rb–Sr dating on fluid inclusions at Jinya and Lannigou has probably given errorchrons that do not provide geochronologic information. The interpretation that the 134–136 Ma Sm–Nd dates of hydrothermal calcite veins at Shuiyindong represent the age of gold deposition (Su et al. 2009b) is probably also suspect because paragenetic relationships indicate that the calcite veining was commonly later than gold mineralization. These Sm–Nd dates probably represent the age of the latest hydrothermal activity but do not provide reliable constraints on the age of the deposit.

Consequently, among the limited isotopic dates that have been reported, the Rb–Sr date on Au-bearing hydrothermal sericite at Jinya (206±12 Ma; Wang 1992) as well as the Re–Os date on auriferous arsenian pyrite (193±13 Ma; Chen et al. 2007) and $^{40}Ar/^{39}Ar$ date on vein-filling sericite (194.6±2 Ma; Chen et al. 2009) at Lannigou may provide the most reliable age constraints on gold mineralization for these deposits. This age range of 206–193 Ma corresponds to the late Triassic (late Indosinian) to early Jurassic (early Yanshanian).

It is commonly difficult to precisely fix the charging ages of hydrocarbon reservoirs because of the absence of datable minerals. Zhou (1999) suggested that the Permian source rocks in the Youjiang basin had reached peak oil-generation stage during 238–235 Ma, and large-scale migration of the oil occurred around 235 Ma. Based on homogenization temperature data of the hydrocarbon-bearing fluid inclusions in the Shitouzhai paleo-oil reservoir, in combination with the thermal evolution history (ancient geothermal gradient) of the Youjiang basin as well as the burial history of the reservoir rocks, Gu et al. (2006, 2007b) estimated the petroleum charging age at Shitouzhai to be between 238 and 185 Ma, corresponding to the middle Triassic to the early Jurassic. The lower end of this age range roughly corresponds to the Sm–Nd isochron age (182±21 Ma) of the pore- and fissure-filling calcite-III associated with bitumen at Shitouzhai obtained in this study (Fig. 8). Therefore, the age range of 238–182 Ma may represent the time of migration for hydrocarbons entering the reservoir and accumulating in a trap and is comparable with the probable age range (206–193 Ma) for gold mineralization at the Jinya and Lannigou gold deposits.

Genetic linkage

In the Youjiang basin, the spatially close association of sedimentary rock hosted gold deposits and paleo-oil reservoirs, the paragenetic coexistence of mobilized organic matter (bitumen) with ore-stage minerals, the presence of abundant hydrocarbons in the ore fluids, and the temporal coincidence of gold mineralization and hydrocarbon accumulation favor a coeval model in which the metals originated, migrated, and precipitated along with the hydrocarbons in an immiscible, ore- and hydrocarbon-bearing, basinal fluid system.

As the products of basinal fluid activities, both metallic ore deposits and hydrocarbon reservoirs experienced similar evolutionary processes. Adequate sources of metals and/or hydrocarbons, suitable media and pathways for migration, and favorable precipitation and/or trap mechanisms are crucial for both mineralization and hydrocarbon accumulation. Some sedimentary rocks enriched in metals and organic matter may have served as the sources for both metallic ore deposits and hydrocarbon reservoirs. Accordingly, some economic geologists (e.g., Tu 1988; Fu et al. 1990) proposed the concept of "dual source layer" to highlight the genetic link between mineralization and hydrocarbon accumulation. During the burial diagenesis of metal- and organic matter-rich sediments, metals could be dissolved in pore waters and expelled along with oil and gases from the source rocks. The simulation experiments by Lu and Zhuang (1996) indicated that during the thermal evolution of "dual-source layer," gold was expelled from the source rock along with crude oil, and the contents of gold in the crude oil ranged between 1.35 and 5.29 ppm.

The experimental study by Williams-Jones and Migdisov (2006) also showed that the solubility of gold in crude oil averaged 9 ppm at 150°C and 14 ppm at 200°C. They concluded that liquid hydrocarbons are capable of transporting ore level and higher concentrations of gold. In southwestern Guizhou Province, the Permian deep-water facies, organic and metal (Au, As, Hg, Sb) rich, black mudrock and carbonaceous limestone are thought to be source rocks for both Carlin-type gold deposits and the Permian reef paleo-oil reservoirs (Shi et al. 1995, 1998; Yang et al. 1999).

Effective driving mechanisms for basinal fluid flow may include: (1) overpressuring caused by compaction of sediments (compaction-driven flow; e.g., Sharp 1978; Bϕjrlykke 1993; Ortoleva 1994; Vearncombe et al. 1996), (2) hydraulic forcing caused by tectonic uplift in a foreland basin (topographically driven flow; e.g., Garven and Freeze 1984; Garven 1989), (3) orogenic compression of the source basin (tectonically driven flow; e.g., Oliver 1986), and (4) petroleum and gas expulsions (Bϕjrlykke 1993; Eisenlohr et al. 1994). In general, overpressuring caused by sediment compaction constrains horizontal fluid migration along aquifers from depocenters followed by vertical fluid flow along the basin- and subbasin-bounding normal faults onto the edges and paleohighs of the basin, where the fluid flow is concentrated. Topographic relief and basin compression may drive the fluid flow from the orogen laterally toward the basinal margin adjacent to the forebulge.

In the Youjiang basin, as described above, the Carlin-type gold deposits and paleo-oil reservoirs are commonly localized either at the margin of the basin or in the intrabasinal paleohighs (carbonate platforms and reefs) near subbasin-bounding syndepositional faults (Fig. 1). It is also noted that the gold deposits and paleo-oil reservoirs occur more commonly near the northwest margin than in the other marginal areas of the basin (Fig. 1; Gu et al. 2007a). Consequently, both compaction-driven and topographically/tectonically driven fluid flows are the likely mechanisms in the Youjiang basin. The overpressuring caused by sediment compaction probably occurred during the late Paleozoic (Hercynian) to middle Triassic (early Indosinian) extension that caused major rifting, rapid subsidence, and sedimentation in the basin, while the topographic relief and basin compression occurred during the late Triassic (late Indosinian) to probably early Jurassic (early Yanshanian) foreland basin period because of the uplift of south and southwest margins of the basin (Zeng 1993; Zeng et al. 1995). The overall spatial distribution of the gold deposits and paleo-oil reservoirs was largely controlled by the basinal fluid flow during these two events.

Focusing of the hydrocarbon- and Au-rich fluids at the basinal margins and paleohighs could have caused both hydrocarbon accumulation and gold mineralization by probably different trapping and depositional mechanisms. Hydrocarbons were accumulated when encountering appropriate stratigraphic, lithologic, and structural traps, such as unconformities, reefs, sandstone lenses, and anticlines. The formation of hydrocarbon traps is thus essentially a physical process and requires a relatively stable environment. In contrast, gold precipitation may have occurred when the upward migrating ore fluids encountered suitable geochemical barriers, by processes such as decrease in temperature and pressure, mixing with cold ground water, replacement with host rocks, and fluid boiling. These processes need an abrupt change in physicochemical conditions. Therefore, the gold deposits and hydrocarbon reservoirs could be spatially separated from each other at the site of deposition to some extent, as demonstrated in this study, although they are confined to the same tectonic units (Fig. 1).

Fluid inclusion data indicate that the temperatures of hydrothermal fluids for the gold deposits in the Youjiang basin typically ranged from 120°C to 270°C (Table 1). The temperatures of hydrocarbon fluids from the paleo-oil reservoirs varied from 73°C to 219°C (mostly from 90°C to 180°C; Table 2), approximately corresponding to the temperature range of peak-oil to condensate oil and wet gas (or even dry gas) generations (e.g., Tissot and Welte 1984; Shi and Yu 1996). This temperature range is roughly in accordance with the lower end of the temperatures for the ore fluids. Such a temperature relationship implies that the hydrocarbons may have been trapped at relatively low temperatures, while the formation of gold deposits could have occurred under a wider and higher range of temperatures. The salinities of ore-forming fluids and paleo-oil reservoir fluids are low and comparable (typically lower than 8 wt% NaCl eq.), consistent to the lack of evaporites in the Youjiang basin.

Based on the foregoing discussion, a possible genetic model for the gold mineralization and hydrocarbon accumulation in the Youjiang basin is illustrated in Fig. 9.

During the rifting period in the late Paleozoic to middle Triassic, the Youjiang basin consisted of a series of isolated platforms separated by subbasins. The boundaries between the subbasins and platforms are marked by NW- and NE-trending syndepositional normal faults. Deep water, organic matter and metal (Au, As, Hg, and Sb) rich mudstone, siltstone, and micrite deposited in the subbasins, which served as sources for the later gold mineralization and hydrocarbon accumulation. Shallow water limestone, biohermal limestone, and locally, siliceous clastic rocks deposited on the platforms and basinal margins, which supplied favorable spaces for the later gold deposition and hydrocarbon accumulation. The basin-bounding and intrabasinal normal faults between subbasins supplied major conduits for the focusing migration of basinal fluids.

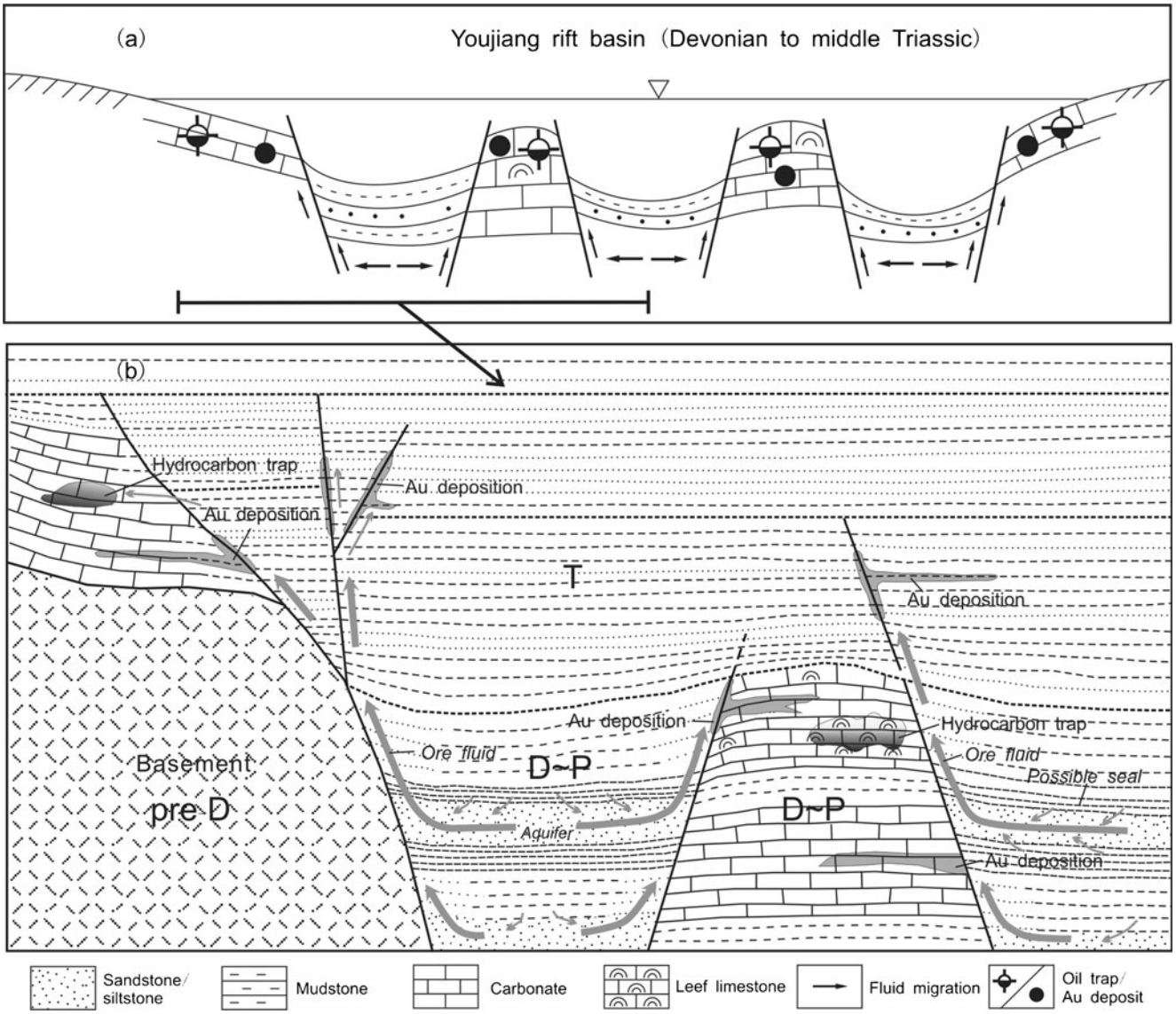

Fig. 9 Schematic presentation of a possible genetic model for gold mineralization and hydrocarbon accumulation in the Youjiang basin. *pre-D* Pre-Devonian; *D-T* Devonian to Triassic; *T* Triassic. See the text for explanation

Gold and hydrocarbons were released into and transported along with pore waters during diagenesis. The gold- and hydrocarbon-bearing fluids, driven by sediment compaction as well as topographic relief and basin compression, migrated horizontally along aquifers and then focused vertically along the basin- and subbasin-bounding normal faults onto the edges and paleohighs of the basin, where the gold mineralization and hydrocarbon accumulation took place. Gold precipitated along faults, fracture zones, and unconformity surfaces where the ore fluids encountered suitable geochemical barriers, while hydrocarbons were accumulated in appropriate stratigraphic, lithologic, and structural traps. Because of the different depositional and trapping mechanisms, the gold deposits and hydrocarbon reservoirs are spatially separate to some extent at the site of deposition and accumulation. The uplift and folding of the Youjiang basin during the Yanshanian orogeny resulted in the exhumation and destruction of most, if not all, hydrocarbon reservoirs, with abundant and widespread bitumens as the only residues left at the surface.

Conclusions

The spatially close association of sedimentary-rock hosted gold deposits and paleo-oil reservoirs in the Youjiang basin, the paragenetic coexistence of mobilized organic matter (bitumen) with ore-stage minerals, the presence of abundant hydrocarbons in the ore fluids, and the temporal coincidence of gold mineralization and hydrocarbon accumulation suggest

that the gold originated, migrated, and precipitated along with the hydrocarbons in an immiscible, gold, and hydrocarbon bearing basinal fluid system. Deep water, organic matter and metal (Au, As, Hg, and Sb) rich mudstone, siltstone, and micrite deposited in the rift basin and served as sources for both the gold deposits and the paleo-oil reservoirs. Gold and hydrocarbons were released into and transported along with pore waters during diagenesis. The gold- and hydrocarbon-bearing fluids migrated horizontally along aquifers and then focused vertically along the basin- and subbasin-bounding normal faults onto the edges and paleohighs of the basin, where the gold mineralization and hydrocarbon accumulation took place by different depositional/trapping mechanisms. Exhumation of the basin during the Yanshanian resulted in the destruction of hydrocarbon reservoirs with bitumens as the only residues left.

Acknowledgment We are grateful to Y. S. Zhai for his helpful suggestions and discussions. The manuscript has been significantly improved from constructive comments by two anonymous reviewers. Insightful handling from B. Lehmann and N. White is also greatly appreciated. The research was funded by the National Natural Science Foundation of China (NSFC) under grants 40930423, 40772060, and 40873036, the 973 National Basic Research Priorities Program (2009CB421003-01), and the Project 111 from the Ministry of Education of China.

References

Anderson GM (1991) Organic maturation and ore precipitation in southeast Mississippi. Econ Geol 86:909–926

Arehart GB (1996) Characteristics and origin of sediment-hosted gold deposits: a review. Ore Geol Rev 11:383–403

Bodnar RJ (1993) Revised equation and table for determining the freezing point depression of H_2O–NaCl solutions. Geochim Cosmochim Acta 57:683–684

Broadbent G, Myers R, Wright J (1998) Geology and origin of shale-hosted Zn–Pb–Ag mineralization at the Century deposit, Northwest Queensland, Australia. Econ Geol 93:1264–1294

Burke EAJ (2001) Raman microspectrometry of fluid inclusions. Lithos 55:139–158

Bϕjrlykke K (1993) Fluid flow in sedimentary basins. Sediment Geol 86:137–158

Cai CF, Dong HL, Li HT, Xiao XJ, Ou GX, Zhang CM (2007) Mineralogical and geochemical evidence for coupled bacterial uranium mineralization and hydrocarbon oxidation in the Shashagetai deposit, NW China. Chem Geol 236:167–179

Cail TL, Cline JS (2001) Alteration associated with gold deposition at the Getchell Carlin-type gold deposit, North-Central Nevada. Econ Geol 96:1343–1359

Carpenter AB, Trout ML, Pickett EE (1974) Preliminary report on the origin and chemical evolution of lead- and zinc-rich oil field brines in central Mississippi. Econ Geol 69:1191–1206

Chen TJ (1986) A preliminary discussion on geological features of Banqi Au deposit in Ceheng. Guizhou Geology 9(4):321–339 (in Chinese)

Chen MH, Mao JW, Qu WJ, Wu LL, Uttley PJ, Norman T, Zheng JM, Qin YZ (2007) Re–Os dating of arsenian pyrites from the Lannigou gold deposit, Zhenfeng, Guizhou Province, and its geological significances. Geol Rev 53:371–382 (in Chinese with English abstract)

Chen MH, Huang QW, Hu Y, Chen ZY, Zhang W (2009) Genetic types of phyllosilicate (mica) and its ^{39}Ar–^{40}Ar dating in Lannigou gold deposit, Guizhou province. China. Acta Mineralogica Sin 29:353–362 (in Chinese with English abstract)

Christensen OD (1993) Carlin trend geologic overview. In: Christensen OD (ed) Gold deposits of the Carlin trend, Nevada. Society of Economic Geologists Guidebook Series, no. 18. Society of Economic Geologists, Littleton pp 12–26

Christensen JN, Halliday AN, Kesler SE, Leigh KE, Randell RN (1995) Direct dating of sulfides by Rb–Sr: a critical test using the Polaris Mississippi Valley-type Zn-Pb deposit. Geochim Cosmochim Acta 59:5191–5197

Christensen JN, Halliday AN, Kesler SE (1997) Rb–Sr dating of sphalerite and the ages of Mississippi Valley-type Pb–Zn deposits. Society of Economic Geologists Special Publication 4:527–535

Cline JS (2001) Timing of gold and arsenic sulfide mineral deposition at the Getchell Carlin-type gold deposit, North-Central Nevada. Econ Geol 96:75–89

Cline JS, Hofstra AH, Muntean JL, Tosdal RM, Hickey KA (2005) Carlin-type gold deposits in Nevada: critical geologic characteristics and viable models. Economic Geology 100th Anniversary Volume, pp 451–484

Curiale JA (1993) Oil to source rock correlation-concepts and case studies. In: Engel MH, Macko SA (eds) Organic geochemistry. Plenum, London, pp 473–490

Eisenlohr BN, Tompkins LA, Cathles LM, Barley ME, Groves DI (1994) Mississippi Valley-type deposits: products of brine expulsion by eustatically induced hydrocarbon generation? An example from northwestern Australia. Geology 22:315–318

Emsbo P, Hutchinson RW, Hofstra AH, Volk JA, Bettles KH, Baschuk GJ, Johnson CA (1999) Syngenetic Au on the Carlin trend: implications for Carlin-type deposits. Geology 27:59–62

Emsbo P, Hofstra AH, Lauha EA, Grifein GL, Hutchinson RW (2003) Origin of high-grade gold ore, source of ore fluid components, and genesis of the Meikle and neighboring Carlin-type deposits, northern Carlin trend, Nevada. Econ Geol 98:1069–1105

Farrell KPJ, Mossman DJ (1994) Origin, mode of emplacement, and trace element geochemistry of albertite at the type locality, Albert Mines, southeastern New Brunswick, Canada. Energy Sources 17:359–371

Fu JM, Peng PA, Lin Q (1990) Some problems concerning study on organic geochemistry of stratabound deposits. In: Shi JY (ed) Annual report of the Open Laboratory of Organic Geochemistry in 1998, Institute of Geochemistry, Chinese Academy of Sciences. Science Press, Beijing, pp 174–185 (in Chinese)

Fu SH, Gu XX, Wang Q, Xia Y, Zhang XC, Tao Y (2004) The typomorphic characteristics of gold-bearing pyrites from the Shuiyindong gold deposit, SW Guizhou. Acta Mineralogica Sin 24:75–80 (in Chinese)

Garven G (1989) A hydrologic model for the formation of the giant oil sands deposits of the Western Canada Sedimentary Basin. Am J Sci 289:105–166

Garven G, Freeze RA (1984) Theoretical analysis of the role of groundwater flow in the genesis of stratabound ore deposits. 2. Quantitative results. Am J Sci 284:1125–1174

Gize AP, Barnes HL (1994) Organic contributions to Mississippi Valley-type lead-zinc genesis-a critical assessment. In: Fontbote L, Boni (eds) Sediment–host Zn–Pb ores. Springer, Berlin–Heidelberg, pp 13–26

Glikson M, Mastalerz M, Golding SD, McConachie BA (2000) Metallogenesis and hydrocarbon generation in northern Mount Isa Basin, Australia: implications for ore grade mineralization. In: Glikson M, Mastalerz M (eds) Organic matter and mineralization: thermal

alteration, hydrocarbon generation and role in metallogenesis. Kluwer Academic, Dordrecht, pp 149–184

Gu XX (1996) Turbidite-hosted micro-disseminated gold deposits. Chengdu University of Science and Technology Press, Chengdu

Gu XX, Liu JM, Schulz O, Vavtar F, Zheng MH (2002) Syngenetic origin for the sediment-hosted disseminated gold deposits in NW-Sichuan, China: ore fabric evidence. Ore Geol Rev 22:91–116

Gu XX, Li BH, Xu SH, Fu SH, Dong SY, Zeng LG (2006) Time coupling of oil-gas reservoir formation and Au mineralization in the Youjiang basin: Sm–Nd isotopic constraints. Mineral Deposits 25 (Suppl):217–220 (in Chinese)

Gu XX, Li BH, Xu SH, Fu SH, Dong SY (2007a) Characteristics of hydrocarbon-bearing ore-forming fluids in the Youjiang Basin, South China: implications for hydrocarbon accumulation and ore mineralization. Earth Sci Frontiers 14:133–146 (in Chinese with English abstract)

Gu XX, Li BH, Xu SH, Fu SH, Dong SY (2007b) Analysis of the charge history of the Shitouzhai Permian paleo-oil reservoir, Guizhou, SW-China: fluid inclusion and Sm–Nd isotope constraints. Acta Petrologica Sin 23:2279–2286 (in Chinese with English abstract)

Gu XX, Zhang YM, Li BH, Xue CJ, Dong SY, Fu SH, Liu L, Wu CY (2010) The coupling relationship between metallization and hydrocarbon accumulation in sedimentary basins. Earth Sci Frontiers 17:83–105 (in Chinese)

Hanor JS (1994) Origin of saline fluids in sedimentary basins. In: Parnell J (ed) Geofluids: origin, migration and evolution of fluids in sedimentary basins. Geological Society Special Publication, no. 78. Geological Society, London, pp 151–174

Henry AL, Anderson GM, Heroux Y (1992) Alteration of organic matter in the Viburnum Trend lead–zinc district of southeast Missouri. Econ Geol 87:288–309

Hofstra AH, Cline JS (2000) Characteristics and model for Carlin-type gold deposits. Reviews in Economic Geology 13:163–220

Hu RZ, Su WC, Bi XW, Li ZQ (1995) A possible evolution way of ore-hydrothermal fluid for the Carlin-type gold deposits in the Yunnan-Guizhou-Guangxi triangle area. Acta Mineralogica Sin 15:144–149 (in Chinese)

Hu RZ, Su WC, Bi XW, Tu GC, Hofstra AH (2002) Geology and geochemistry of Carlin-type gold deposits in China. Miner Deposita 37:378–392

Hulen JB, Collister JW (1999) The oil-bearing, Carlin-type gold deposits of the Yankee basin, Alligator Ridge district, Nevada. Econ Geol 94:1029–1049

Hulen JB, Pinnell ML, Nielson DL, Cox JW, Blake J (1994) The Yankee mine oil occurrence, Alligator Ridge district, Nevada-an exhumed and oxidized, paleogeothermal oil reservoir. In: Schalla RW, Johnson EH (eds) Oil fields of the Great Basin. Nevada Petroleum Society, Reno, pp 131–149

Huston DL, Stevens B, Southgate PN, Muhling P, Wyborn L (2006) Australian Zn–Pb–Ag ore-forming systems: a review and analysis. Econ Geol 101:1117–1157

Ilchik RP, Brimhall GH, Schull HW (1986) Hydrothermal maturation of indigenous organic matter at the Alligator Ridge gold deposits, Nevada. Econ Geol 81:113–130

Johansson L, Kullerud L (1993) Late Sveconorwegian metamorphism and deformation in southwest Sweden. Precam Res 64:347–360

Kesler SE, Jones HD, Furman FC, Sassen R, Anderson WH, Kyle JR (1994) Role of crude oil in the genesis of Mississippi Valley-type deposits: evidence from the Cincinnati arch. Geology 22:609–612

Kesler SE, Campbell IH, Smith CN, Hall CM, Allen CM (2005) Age of the Pueblo Viejo gold-silver deposit and its significance to models for high-sulfidation epithermal mineralization. Econ Geol 100:253–272

Lee MK, Williams DD (2000) Paleohydrology of the Delaware basin, western Texas: overpressure development, hydrocarbon migration, and ore genesis. AAPG Bull 84:961–974

Leventhal J, Hofstra A (1990) Characterization of carbon in sediment-hosted disseminated gold deposits, north central Nevada. In: Hausen DM, Halbe DN, Petersen EU, Tafuri WJ (eds) Gold'90. Society for Mining, Metallurgy, and Exploration, Littleton. pp 365–368

Li WK, Jiang XS, Ju RH, Mang FY, Zhang SX (1989) The characteristics and metallogenic process of disseminated gold deposits in Southwest Guizhou. Proceeding of regional metallogenic conditions about main types of Chinese gold deposits vol 6. Geological Publishing House, Beijing, pp 1–86 (in Chinese)

Lin Q, Liu DH (1995) Organic geochemical study of gold deposits in southwestern Guizhou Province. Geochimica 24:402–408 (in Chinese)

Liu JZ, Liu CQ (2005) Origin and metallogenic model for Shuiyindong gold deposit of Guizhou. Guizhou Geology 22:9–13 (in Chinese)

Lu JL, Zhuang HP (1996) Experimental studies on role of organic matter during mineralization of gold and silver at low temperatures. Geochimica 25:172–180

Liu DS, Tan YJ, Wang JY, Wei LM (1994) Carlin-type gold deposits in China. In: Liu DS, Tan YJ, Wang JY, Jiang SF (eds) Chinese Carlin-type gold deposits. Nanjing University Press, Nanjing, pp 1–36 (in Chinese)

Liu JM, Ye J, Ying HL, Liu JJ, Zheng MH, Gu XX (2002) Sediment-hosted micro-disseminated gold mineralization constrained by basin paleo-topographic highs in the Youjiang basin, South China. J Asian Earth Sci 20:517–533

Luo XH (1994) Geological characteristics, forming mechanism and prospect on Lannigou gold deposit in Zhengfeng County, Guizhou Province. In: Liu DS, Tan YJ, Wang JY, Jiang SF (eds) Chinese Carlin-type gold deposits. University of Nanjing Press, Nanjing, pp 100–115 (in Chinese)

Montacer M, Disnar JR, Orgeval JJ, Trichet J (1988) Relationship between Zn-Pb ore and oil accumulation processes: example of the Bou Grine Deposit (Tunisia). Org Geochem 13:423–431

Mossman DJ (1999) Carbonaceous substances in mineral deposits: implications for geochemical exploration. J Geochem Expl 66:241–247

Nutt CJ, Hofstra AH (2003) Alligator Ridge district, east-central Nevada: Carlin-type gold mineralization at shallow depths. Econ Geol 98:1225–1241

Oliver J (1986) Fluids expelled tectonically from orogenic belts: their role in hydrocarbon migration and other geologic phenomena. Geology 14:99–102

Ortoleva PJ (1994) Basin compartments and seals. Developments in Petroleum Sciences 9. Elsevier, Amsterdam, pp 1–45

Parnell J (1988) Metal enrichments in solid bitumens. Miner Deposita 23:191–199

Peabody CE (1993) The association of cinnabar and bitumen in mercury deposits of the California Coast Ranges. In: Parnell J, Kucha H, Landais P (eds) Bitumen in ore deposits. Springer, Berlin, pp 178–209

Peabody CE, Einaudi MT (1992) Origin of petroleum and mercury in the Culver-Baer cinnabar deposit, Mayacmas district, California. Econ Geol 87:1078–1103

Peters SG, Huang JZ, Li ZP, Jing CG (2007) Sedimentary rock-hosted Au deposits of the Dian-Qian-Gui area, Guizhou, and Yunnan provinces, and Guangxi district, China. Ore Geol Rev 31:170–204

Presnell R (1993) The association of gold and hydrocarbons in sediment-hosted disseminated gold deposits [abs]. AAPG Bull 77:1459

Radtke AS (1985) Geology of the Carlin gold deposit, Nevada. US Geological Survey Professional Paper 1267:124p

Radtke AS, Scheiner BJ (1970) Studies of hydrothermal gold deposition (I). Carlin gold deposit, Nevada: the role of carbonaceous materials in gold deposition. Econ Geol 65:87–102

Rieger A, Schwark L, Cisternas ME, Miller AH (2008) Genesis and evolution of Bitumen in Lower Cretaceous lavas and implications for strata-bound copper deposits, North Chile. Econ Geol 103:387–404

Sharp JM (1978) Energy and momentum transport model of the Ouachita basin and its possible impact on formation of economic mineral deposits. Econ Geol 73:1057–1068

Shepherd TJ, Rankin AH, Alderton DH (1985) A practical guide to fluid inclusion studies. Blackie and Son, Glasgow

Sherlock R (2000) The association of gold-mercury mineralization and hydrocarbons in the coast ranges of northern California. In: Glikson M, Mastalerz M (eds) Organic matter and mineralization: thermal alteration, hydrocarbon generation and role in metallogenesis. Kluwer Academic Publishers, Dordrecht, pp 378–399

Shi JX, Yu XY (1996) Characteristics of organic matter in carbonate rocks and unconventional evaluation of oil and gas. Acta Mineralogica Sin 16:103–108 (in Chinese)

Shi JX, Yu XY, Wang HY (1995) The role of ancient reservoirs, bitumens, and bitumen inclusions in metallogenetic research. Acta Mineralogica Sin 15:117–122 (in Chinese)

Shi JX, Wang HY, Lin Q (1998) Low temperature Au, Sb, and Hg mineralization and its relation to organic matter. In: Tu GC (ed) Low temperature geochemistry. Science, Beijing, pp 53–76 (in Chinese)

Spangenberg JE, Macko SA (1998) Organic geochemistry of the San Vicente zinc-lead district eastern Pucara Basin, Peru. Chem Geol 146:1–23

Spirakis CS, Heyl AV (1992) Organic matter (bitumen and other forms) as the key to localisation of Mississippi Valley-type ores. In: Parnell J, Kucha H, Landais P (eds) Bitumen in ore deposits. Springer, Berlin, pp 381–398

Su WC (2002) Geochemistry of the ore-forming fluids of the Carlin-type gold deposits in the southwestern margin of the Yangtze block. Dissertation, Institute of Geochemistry, Chinese Academy of Sciences, Guiyang (in Chinese)

Su WC, Xia B, Zhang HT, Zhang XC, Hu RZ (2008) Visible gold in arsenian pyrite at the Shuiyindong Carlin-type gold deposit, Guizhou, China: implications for the environment and processes of ore formation. Ore Geol Rev 33:667–679

Su WC, Heinrich CA, Pettke T, Zhang XC, Hu RZ, Xia B (2009a) Sediment-hosted gold deposits in Guizhou, China: products of wall-rock sulfidation by deep crustal fluids. Econ Geol 104:73–93

Su WC, Hu RZ, Xia B, Xia Y, Liu YP (2009b) Calcite Sm–Nd isochron age of the Shuiyindong Carlin-type gold deposit, Guizhou, China. Chem Geol 258:269–274

Sun YZ, Püttmann W (2000) The role of organic matter during copper enrichment in Kupferschiefer from the Sangerhausen basin, Germany. Org Geochem 31:1143–1161

Sverjensky DA (1984) Oil field brines as ore-forming solution. Econ Geol 17:23–37

Tao CG (1990) Ore-controlling factors and exploration guides of superfine-grained disseminated gold deposits, southwestern Guizhou. Geology and Prospecting 26(8):9–15 (in Chinese)

Tissot BP, Welte DH (1984) Petroleum formation and occurrence. Springer, New York

Tu GC (1988) Geochemistry of stratabound ore deposits in China, vol 3. Science, Beijing (in Chinese)

Tu GC (1994) The relationship between coal-, oil- and gas-accumulation and metal mineralization. Geological Exploration for Non-Ferrous Metals 3(1):1–3 (in Chinese)

Vearncombe JR, Chisnall AW, Dentith M, Dörling S, Rayner MJ, Holyland PW (1996) Structural controls on Mississippi Valley-type mineralization, the southeast Lennard shelf. Society of Economic Geologists Special Publication no. 4. Society of Economic Geologists, Perth, pp 74–95

Wang GT (1992) Three strontium–rubidium isochron ages in northwest Guangxi. Geology of Guangxi 5(1):29–35 (in Chinese)

Wang GZ, Hu RZ, Su WC, Zhu LM (2002) Fluid flow and ore mineralization in the Nanpanjiang basin in Yunnan, Guizhou and Guangxi provinces. Sci China D 32(Suppl):78–86 (in Chinese)

Williams-Jones AE, Migdisov AA (2006) An experimental study of the solubility of gold in crude oil: implications for ore genesis. Geochim Cosmochim Acta, Goldschmidt Conference Abstracts, A703

Wilson NSF, Zentilli M (2006) Association of pyrobitumen with copper mineralization from the Uchumi and Talcuna districts, central Chile. Int J of Coal Geol 65:158–169

Wilson NSF, Zentilli M, Spiro B (2003) A sulfur, carbon, oxygen, and strontium isotope study of the volcanic-hosted El Soldado manto-type Cu deposit, Chile: the essential role of bacteria and petroleum. Econ Geol 98:163–174

Xia Y (2005) Characteristics and model for Shuiyindong gold deposit in southwestern Guizhou, China. Dissertation, Institute of Geochemistry, Chinese Academy of Sciences, Guiyang (in Chinese)

Xue CJ, Chi GX, Qing HR (2007) Organic petrology and geochemistry of the giant Jinding deposit, Lanping basin, northwestern Yunnan. China Acta Petrologica Sin 23:2889–2900 (in Chinese with English abstract)

Yang HM, Liu BW, Deng ZH (1999) Evaluation and selection to the best gas-oil keeping units of marine carbonate area in Yunnan. Guizhou Publishing House of Science and Technology, Guiyang, Guizhou and Guangxi (in Chinese)

Yao ZY (1990) Tectonic-palaeogeographic control of sediment reformed gold deposits in China. Bulletin of the Nanjing Institute of Geology and Mineral Resources. Chinese Academy of Geological Sciences 11(2):87–93 (in Chinese)

Ye XX, Wan GQ, Sun ZY, Liu YK, Zhou LD, Liu SR, Xue DJ, Rivers L, Jones KW (1994) Microbeam analysis of gold in Carlin-type gold deposits, southwestern Guizhou. China Sci China B 24:883–889 (in Chinese)

Zeng YF (1993) Sedimentary and tectonic evolution of the Youjiang basin, South China. Geological Publishing House, Beijing (in Chinese)

Zeng YF, Liu WJ, Chen HD, Zheng RC, Zhang JQ, Li XQ, Jiang TC (1995) Sedimentary and tectonic evolution of the Youjiang composite basin. Acta Geologica Sin 69:113–124 (in Chinese)

Zhang JL (1994) On the relation between the oil and uranium deposits. J East China Geol Int 17:42–45 (in Chinese)

Zhang HT, Su WC, Tian JJ, Liu YP, Liu JZ, Liu CQ (2008) The occurrence of gold at Shuiyindong Carlin-type gold deposit. Guizhou Acta Mineralogica Sin 28:17–24 (in Chinese)

Zhao MJ, Zhang SC, Zhao L, Jiang DA (2007) Geochemical features and genesis of the natural gas and bitumen in paleo-oil reservoirs of Nanpanjiang basin, China. Sci China D 50:689–701

Zhou MH (1999) A study on the petroleum system of the Nanpanjiang sag. Geology of Yunnan 18:248–265 (in Chinese)

Zhuang HP, Lu JL, Fu JM, Ren CG, Zou DG (1999) Crude oil as carrier of gold: petrological and geochemical evidence from the Lannigou gold deposit in southwestern Guizhou, China. Sci China D 42:216–224